Microchimica Acta (2022) 189: 127
https://doi.org/10.1007/s00604-022-05228-2

REVIEW ARTICLE

Wearable electrochemical biosensors to measure biomarkers with complex blood-to-sweat partition such as proteins and hormones

David Pérez[1] · **Jahir Orozco**[1]

Received: 2 November 2021 / Accepted: 14 February 2022 / Published online: 1 March 2022

Abstract

Smart electronic devices based on micro-controllers, also referred to as fashion electronics, have raised wearable technology. These devices may process physiological information to facilitate the wearer's immediate biofeedback in close contact with the body surface. Standard market wearable devices detect observable features as gestures or skin conductivity. In contrast, the technology based on electrochemical biosensors requires a biomarker in close contact with both a biorecognition element and an electrode surface, where electron transfer phenomena occur. The noninvasiveness is pivotal for wearable technology; thus, one of the most common target tissues for real-time monitoring is the skin. Noninvasive biosensors formats may not be available for all analytes, such as several proteins and hormones, especially when devices are installed cutaneously to measure in the sweat. Processes like cutaneous transcytosis, the paracellular cell–cell unions, or even reuptake highly regulate the solutes content of the sweat. This review discusses recent advances on wearable devices based on electrochemical biosensors for biomarkers with a complex blood-to-sweat partition like proteins and some hormones, considering the commented release regulation mechanisms to the sweat. It highlights the challenges of wearable epidermal biosensors (WEBs) design and the possible solutions. Finally, it charts the path of future developments in the WEBs arena in converging/emerging digital technologies.

Keywords Electrochemical biosensor screen-printed electrode (SPE) · Field-effect transistor (FET) · Electrochemical impedance spectroscopy (EIS) · Wearable technology · Nanostructures · Protein hormone sweat skin

Introduction

Smart electronic devices, based on micro-controllers, allowed the raising of wearable technology, also referred to as fashionable, mounting, or patchable electronics. In close contact with any surface of the body, these devices may process physiological information facilitating the immediate biofeedback to the wearer. The stated technology became possible in the mid-'90 s when works like the Canadian inventor Steve Mann described his wearable multimedia computer/personal visual assistant [1]. By that time, he dreamed of the moment when "wearable computer systems will be owned, operated, and controlled by the wearer -much like one's own clothes," but just until the early 2000s, mini-wearable cameras were introduced to the market, and at 2010 the first step-counter was launched [2], which has been proposed even in the clinical context as a pedometer replacement device [3].

Standard market wearable devices detect observable or electrophysical signs, e.g., gesture, voice, strain, temperature, heart rate, or skin conductivity [4–6].

Contrastingly, the technology that relies on electrochemical biosensors detects soluble analytes associated with a specific disease or condition, also called biomarkers. The most critical feature to collect biometric data is the noninvasive formats for real-time physiological monitoring through wearable technology. For the noninvasiveness, it is required direct sampling of any biofluid to contact the biomarker with the biosensing device. Then, sweat is the most plausible fluid for this purpose. Sampling the skin is less risky and more comfortable for implantation than blood vessels, organs, eyes, mouth, or urinary tract.

✉ David Pérez
djose.perez@udea.edu.co

✉ Jahir Orozco
grupotandem.nanobioe@udea.edu.co

[1] Max Planck Tandem Group in Nanobioengineering, Institute of Chemistry, Faculty of Natural and Exact Sciences, University of Antioquia, Complejo Ruta N, Calle 67, Nº 52-20, 050010 Medellín, Colombia

While it is easy to be held and put the wearable biosensor in near contact with the skin, simple designs may ensure rapid sweat transport to the detection zone. At the same time, a continuous response may be recorded without important harmful consequences in most people [7]. Immediately processing it is also advantageous because it avoids the sample loss and false analytes levels alterations through evaporation or the degradation by self-local mechanisms, such as proteases or commensal microbiota.

Semiconductor microfabrication, soft electronics, and robotic sensors for pressure and thermal distribution are the three pillars for the "smart-skin" development, also known as "electronic" or "synthetic" skin [6, 8]. An explosion of reports has tried to improve smart-skin technology with wearable epidermal biosensors (WEBs) in recent years. Most WEBs use sweat to detect ions, e.g., Cl^-, Na^+, K^+ or metabolites, e.g., glucose, lactate, uric acid. Since the blood-to-sweat partition complexity of proteins and some hormones, the basal levels remain undetermined and WEBs are lesser used to monitoring those potential biomarkers.

Electrochemical WEBs are challenged by the necessity to measure the electric changes of the system continuously and in a real-time manner, according to the analyte's levels. These measuring platforms combine the high selectivity and specificity of bioreceptors with surface electrochemistry. The biorecognition event is further detected by platforms relying on transistors or electrochemical cells and transduced to estimate the analyte's level [12].

In the past two decades, the advance in nanomaterials development and basic research on sweat biology has enabled a slight but firm spreading of the mentioned device's usage to monitor some proteins and hormones as potential biomarkers [13]. For instance, different nanomaterials have been incorporated into the devices depending on the shape and material distribution in different dimensions, including zero-dimensional (0D) (e.g., quantum dots), 1D (e.g., nanowires), 2D (e.g., graphene) and 3D (e.g., nanospheres) [14]. Significantly, the reduced surface-to-bulk ratio of classical devices based on semiconductors as Si and oxides like Ta_2O_5 or Al_2O_3, were challenged by the nano-sized version of the same materials or others like graphene [15]. For example, nanowires (MNWs) are 1D anisotropic filled cylindrical structures that can be made with metallic or semiconducting materials maintaining a large surface area-to-volume ratio, which in turn means a lower detection potential (high electrocatalytic efficiency) and high sensitivity, e.g., high currents [14]. Likewise, van der Waals (vdW) materials, such as graphene and indium selenide, are made of covalent 2D layers, stabilized in their third dimension through weaker vdW forces (i.e., dipole–dipole, dipole-induced dipole and London or dispersion forces). vdW materials have shown features that may also overcome the quoted sensitivity issue [16–18]. Graphene is a vdW nanomaterial that may be customized according to thickness, bandgap, and electronic confinement requirements, permitting its use as a transducer. The sp^2 hybridization of graphene lattices allows it to be chemically inert and confers a behavior like an intrinsic semiconductor or even as a semimetal [19]. It allows easy charge mobility, but the graphene conductivity is significatively sensitive to the electrostatic changes in the surrounding microenvironment [20]. As proof, the carrier mobility capacity of graphene sheets measured in electrolyte-gated Hall bar, with contacts made of Cr/Au and capped in SiO_2, showed almost equal mobility values compared with benchmark SiO_2-supported graphene devices (i.e., ~ 7000 cm^2/Vs), suggesting a robust electrical capacity of graphene, even in an aqueous electrolyte environment [21].

Recent reviews give a comprehensive introduction to the techniques used to design and fabricate flexible biosensors for sweat-based health or exercise monitoring [22], including the devices based on electrochemical cells and transistors [23]. Here, we discuss and compare the essential functioning and analytical elements of electrochemical WEBs in the quoted formats. Seminal works that did allow the apparition of the "smart-skin" from 2011 are also commented. We analyzed them from a molecular point of view that explains the complexity of blood-to-sweat partition like proteins and some hormones. In this context, we describe the main sweat formation mechanisms that compartmentalize the quoted molecules compared to both the blood or interstitial fluid (ISF) and the ideal conditions for sampling it onto WEBs. The importance of basic research in fields as metabolomics and proteomics to identify new and more specific protein biomarkers is stressed. In comparison with a pathological release, intelligent devices that may learn and discriminate the basal release of protein analytes associated with the mere presence of biosensors onto the skin are discussed. Finally, we comment on the plausibility of noninvasive WEBs for large specific protein and how the internet-of-things (IoT), artificial intelligence (AI), and deep learning (DL) intricate to fabricate them according to the REASSURED criteria, i.e., real-time, ease sample collection, affordable, sensitive, specific, user-friendly, rapid, equipment-free and delivered devices.

Sweat gland physiology and WEB's sweat sampling

Skin belongs to the barrier's mechanisms from the innate immunosystem. The cell–cell interactions between keratinocytes avoid the entrance of potential pathogens and the loss of liquid and other components. Altogether, sebaceous glands, hair follicles, and sweat glands are considered skin appendages because they are tissues formed from the down growth of epidermal epithelium during development.

The different ontology from the epidermis [24] explains the absence of appendages like sweat glands in tissue-engineered skin [25]. There are two types of sweat glands, eccrine and apocrine, but some studies suggest a third type called apoeccrine [26–28]. The eccrine gland empties the synthetized sweat directly onto the epidermis, while the apoeccrine usually finishes into the hair follicle and produces a mix that contains carbohydrates, lipids, and proteins [27, 28]. Apocrine sweat glands have a restricted distribution, e.g., anus, external genitalia, nipple of the mammary gland, areola, and axilla. Except for the lips and part of the external genitalia, eccrine is independent, being spread by the whole body (i.e., ~ 3 million, > 100 glands/cm^2, ~ 250–550 glands/cm^2 palms and soles) [28]. The secretory portion of the gland delivers the sweat either directly into the gland's lumen or using the intercellular canaliculi that open to the lumen. Duct segment resorpts part of Na^+ and water, resulting in a hypotonic solution with traces of several types of proteins, amino acids, and other components (Fig. 1a) [29, 30]. While the end tubular segments of the gland are in contact with the outermost layer of the skin, the high amino acid content observed on the sweat has been associated with contamination from degraded epidermal detritus [31]. Finally, the liquid reaches the sweat pore (20–60 µm) through the acrosyringium, the intra-epidermal part of the gland (Fig. 1a). The hydrostatic pressure generated in the gland had been estimated to be 69 kN/m^2 with a sweat rate of 1–20 nL/min/gland and a maximum volume of 8 nL/gland [7, 32]. Molecularly, the sweat formation is initiated by STIM/Orai, two controllers of the intracellular Ca^{2+} levels (Fig. 1a, left) [28, 33]. An analysis of the transcriptome and the proteome from the human eccrine sweat glands did stress the critical role of ionic channels and transporters in the secretory mechanisms [34]. The study also advocates that the nonselective calcium channel called transient receptor potential vanilloid-type 4 (TRPV4) is present in the sweat eccrine gland, suggesting an essential role in wound healing because of its natural contribution to cell–cell junction development [34]. Proteins' size suggests that the associated transport mechanism is neither diffusion nor advection. In contrast, sweat's proteins are secreted by active cellular processes. For instance, basolateral-to-apical transcytosis may transport the protein from the blood to the liquid between tissue cells, known as interstitial fluid (ISF) [7]. Exocytosis, also termed merocrine secretion, may occur at eccrine sweat glands [26]. The exocytic mechanism mobilizes the cytoplasmic vesicles to sites on the plasma membrane, where the vesicular content is released to the extracellular space. On the other hand, the apical part of cells, at the apocrine sweat glands, are pinched off, leading to the release of the cytoplasm and cell membrane joined to the secretory materials (e.g., glycoproteins) [35]. Thus, the protein's partition rate into the sweat will be slower than ions. Note that just a continuous monitoring platform that tests permanently and in "real-time" the local release of sweat will be enough for biosensing through WEBs, because it will avoid the background introduced by contaminants from the epidermis, production, degradation, or concentration after sweat evaporation [7, 26]. Once the WEBs reach a permanent regeneration for continuous and real-time monitoring, these devices could contribute to basic research about the biology of the release mechanisms during sweating.

Eccrine sweat glands respond to heat and stress being stimulated by acetylcholine from the parasympathetic portion of the autonomic system, i.e., cholinergic or muscarinic. Apocrine glands respond to the sensory stimuli but not to heat and are stimulated sympathetically by catecholamines or adrenergic transmitters, i.e., adrenaline and noradrenaline. Briefly, sweating is happening in two ways, thermoregulatory or emotionally. Cholinergic pathways control the sweat-based thermoregulation, starting at forehead, scalp, and face, spreading to the rest of the body, and ending at palms and soles. In contrast, adrenergic regulation is started during emotional stress, and the sweating begins in the palms, soles, and axillae (Fig. 1a). The mean sweat rate per gland remains relatively unchanged with increases in exercise intensity. Distinctly, the whole-body sweat rate increases because the number of recruited active sweat glands grows with exercise [32]. Each gland may reach ~ 20 nL/min during intensive exercise or hard work, which could differ according to the body part [32]. During sweating testing, the quantity of produced sweat and the evaporation is a critical variable that affects the concentration. Analytes like lactate undergo increased production and excretion rate at highly intensive exercise, but its concentration in the total produced sweat decreases, probably because of a dilutional effect [36]. The phenotype also shows intra/interindividual variability, explaining the recommendation for a personalized fluid replacement strategy to achieve high performance in athletes [37]. Likewise, the sweat composition varies according to the diet and acclimation status. A study in humans suggests that a high salt diet (i.e., 6 g of salt per day added to their regular diet during 5 days) did increase the sweat sodium concentration from 39.9 ± 22.5 to 49.7 ± 19.9 mmol/l, compared to low salt diet participants (i.e., 5 days of their regular diet) [38]. Equated to the increase in the urinary sodium excretion (i.e., from 43.2 ± 30.2 mmol to 230.7 ± 89.1 mmol, respectively), sweat sodium levels under two diet regimes undergoes a modest increase [38]. Thus, a possible regulatory role of sweat production in maintaining sodium homeostasis in humans could be proposed [38]. Similarly, the measurement of sodium in sweat from manual outdoor workers has shown higher levels in winter (i.e., 63.8 mmol/L) than in summer (i.e., 44.7 mmol/L) because of the acclimatization process [39]. The heat acclimatization in healthy male volunteers trained by ten days showed a decrease in sweat sodium ion

concentration, suggesting increases in sodium reabsorption capacity [40].

As we had been discussed, it is worth noticing that sweat is obtained from ISF that surrounds the eccrine gland, but most of its components are partitioned compared with the blood and even with ISF (Fig. 1a). Additionally, there is neither a consensus about the "normal" levels of sweat proteins nor about their complete identities. Instead, most of the studies compare the protein levels recorded in apparently healthy individuals. The predictions made by gene ontology have grouped the sweat proteins into two main categories in healthy individuals, catalytic (~40%) and binding (~40%) [29, 41–43]. Dermcidin tends to be the most abundant sweat protein, which, together with apolipoprotein D, clusterin, prolactin-inducible protein, and serum albumin, make up 91% of secreted sweat proteins in healthy individuals [41]. When sweat from eccrine glands is measured, it is difficult to separate the locally produced proteins, those produced in different moments or situations (e.g., emotional vs. heat stress), and avoid sweat mixing from other surfaces or even from apocrine glands. For example, a proteome analysis had been reported just 121 common proteins between eccrine

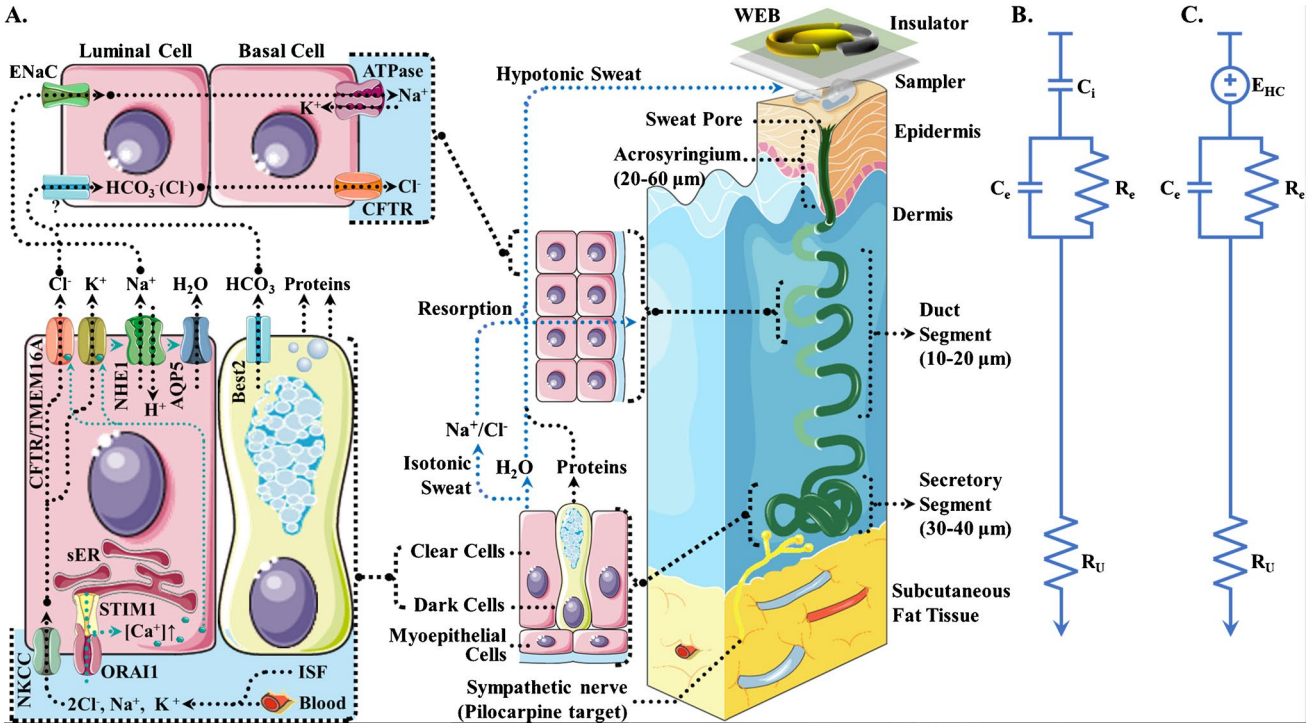

Fig. 1 In steady state of sweat gland (a), the clear cells cumulate Cl^- by the $Na^+/K^+/2Cl^-$ (NKCC) electroneutral co-transporter. After a cholinergic (e.g., temperature, exercise) or adrenergic (stress) stimulus, intracellular Ca^{2+} levels into the clear cells increase by the action of store-operated Ca^{2+} channels (SOCC), controlled by both stromal interaction molecule 1 (STIM1), at the smooth endoplasmic reticulum (sER), and ORAI1 in the plasma membrane. Then, luminal getting out of both Cl^- and K^+ through is carried out. The former is expulsed by the cystic fibrosis transmembrane conductance regulator (CFTR) and transmembrane member 16A (TMEM16A). Since a luminal electrochemical transmembrane gradient is formed, it drags out the Na^+ first and water after, probably by the action of a sodium/hydrogen exchanger (NHE1) or V-Type H^+-ATPase, and the aquaporin 5 (AQP5), respectively. The dark cells send their proteinaceous content to the lumen in a merocrine manner by exocytosis. Here, the HCO_3^- release, by the bestrophin-2 (Best2)-like channels, is shown only in dark cells but also occurs in the clear cells, probably by a SOCC-type regulation. Thus, the isotonic watery component is mixed with the bit of understood glycoproteic secretion. The stratified cuboidal epithelium duct segment resorpts the Na^+/Cl^- passively by the epithelial sodium channel (ENaC) and transporters for HCO_3^-/Cl^- on luminal cells by a less-understood mechanism. Then, the Na/K-ATPases type channels and the CFTR on the basolateral membrane pump the stated ions into the ISF, explaining the sweat hypotonicity concerning the blood. Sweat contains ions (e.g., Na^+, K^+, Ca^+, Mg^{2+}, Cl^-, HCO_3^-) metabolites (e.g., glucose, amino acids, urea, uric acid, and ammonia), hormones (e.g., cortisol), cytokines, immune proteins (e.g., dermcidin, LL-37, cysteine proteinases, cysteine-rich secretory protein-3, DNAse I, lysozyme, Zn-α2-glycoprotein), along with xenobiotics (e.g., drugs, ethanol). Inner diameters of the different portions of the sweat gland are shown. When a chemical WEB is coupled to electrophysiological monitoring, the contact between the skin surface and the electrode can be described by series and parallel combinations of half-cell potentials (E_{HC}), resistors, and capacitors elements. In the case of the dry-insulated WEBs (b) the contribution of insulator is represented by a capacitor C_i followed by a parallel arrangement of an epidermal resistor (R_e) and capacitor (C_e), connected to the resistor of the underlying tissues (R_u). For the penetrating format (c), the E_{HC} is stablished on the needles and its surroundings, while the other electrical elements are represented similarly from the dry insulated. The equivalent circuits are based on [9–11]. Some images were taken modified from free smart server medical art

gland tissue and the sweat, but 28 proteins that are present in the sweat were not present in the eccrine gland tissue, implying the blood, ISF, or even de novo local synthesis, as possible sources [34]. Researches also suggested that the lumen gland transport at apocrine glands of some odor volatile molecules like E-3-methyl-2-hexenoic acid are carried out by unique apocrine proteins like apocrine secretion odor-binding proteins (ASOB) [26, 44]. After exercise, the sweat from either apocrine or eccrine glands has a different composition [45, 46]. Besides, the protein content of sweat after strenuous exercise is different according to gender. A study reported 562 common proteins, while 198 were male and 101 were unique proteins in female pools [47]. Sweat after exercise is rich in hydrolases (53%), but also the singly charged peptides are abundant, suggesting that the high levels of proteolytic enzymes could degrade the other proteins, partially explaining the commented differences [29]. Importantly, whether the commented above report is associated with proteolysis due to the sample handling or innate immune peptides needs to be further defined [29]. Since proteases inhibitors as cystatins and Lymphoepithelial Kazal-type-related inhibitor (LEKTI) were also abundant in sweat after exercise, distinct peptide patterns can occur, depending on the activity balance among them and/or their inhibitors [47]. Individuals diagnosed with schizophrenia showed that 17 proteins at least were increased twofold or greater than healthy individuals [42].

Interestingly, dermcidin showed no differential abundance between sweat from patients with schizophrenia and control ones. Meanwhile, prolactin-binding protein showed a higher abundance in the control individuals. The sweat proteomics from active tuberculosis (aTB) patients had been identified enrichment of proteins with immune (e.g., complement and antibody components), transport (e.g., lipopolysaccharide-binding protein), and enzyme regulation (e.g., trypsin inhibitor) functions [48]. Differential secretion of ribosome components in sweat from aTB patients was also reported, compared with healthy ones [48]. Exosomes are bilayer membrane structures produced at the endosomal cell and released at extracellular space. A proteomic study reported 997 different proteins into exosomes compared with sweat proteomics and 896 unique proteins that were not found in urine, saliva, and plasma exosomes [43]. Sweat´s exosomes are rich in immune proteins like defensins, cathelicidins, immunoglobulins, and cytokines, suggesting a central role of exosomes in skin immunity. Additionally, while the sweat for exosomes harvesting probably belongs to eccrine, apocrine, and apocrine mixed secretion, the absence of contaminant from the holocrine secretion of the sebaceous gland, corneocyte, or bacteria was guaranteed [43].

The proteomic studies covered so far also identify that proteins in sweat are not present in the serum, suggesting that the sweat is not a merely plasma transudate and may contain potential biomarkers that are not present in the blood [42]. While more studies are necessary to determine the standard or basal levels of proteins in the sweat according to the activity level and the type of sweat gland that produces it, all the commented researches suggest that the ideal sweat sample should come from a unique type of sweat gland. The significant quantity of secreted sweat comes from eccrine glands [35], probably the best candidates to be tested.

Since the skin's complexity and dielectric behavior, some researchers suggest it behaves like a barrier instead of a source to collect information deep in the organism [49]. The last is especially true for electrophysiological monitoring, being necessary to consider equivalent circuits (Fig. 1b, c) [9–11]. The redox reactions in the interphase of WEB and the sweat mediate the electrical transport for the readout. During WEB recording, an electrical-double layer (EDL) is formed at each implied surface, leading to a capacitive component at either the insulator or epidermis. Similarly, the skin's components like sebum, epidermal cell–cell unions, and underlying fat explain its high opposition to the current flow, which may be fitted in an equivalent circuitry through a resistor element (Fig. 1b, c) [9–11]. Dry surface WEB does not use conductive gel to be applied. High skin humidity/hydration level reduces the overall skin impedance. So, the built-up perspiration at the skin under WEB will increase the conductivity and the dielectric constant, leading to an overall skin impedance reduction [10]. Thus, the epidermal impedance may be represented by a parallel-connected capacitor (C_e) and resistor (R_e), as shown in Fig. 1b [10, 11]. The transdermal electrode has microneedles embedded into the conductive layers of the epidermis. So, transdermal WEB is well characterized by a half-cell potential (E_{HC}), a capacitor in parallel with a resistor, and an end in series resistance that represents the underlying fat tissues (Fig. 1c) [9–11].

In contrast with the concept of the skin as an electrophysiological monitoring barrier, the potential biochemical biomarkers present in the sweat may be a helpful sample. There is evidence that the protein biomarkers levels variates in the sweat, according to situations or age, in a similar manner as occurs in the blood, keeping apart the cited differences between eccrine and apocrine sweat content. Noninvasive patches and other harvesting systems have been used to obtain sweat and demonstrate this correlation. For instance, levels of cytokines showed a good correlation in a healthy woman, i.e., IL1α, IL-1β, IL-6, TNF-α, IL-8, TGF-β [50] and older adults, i.e., IL-6, IL-10, TNF-α [51], as similarly as cortisol from sweat behaves during exercise [52], heating [53], stress or nutritional challenges [54]. The last is also true when the quoted above analytes are sensed electrochemically in a continuous real-time manner by a wearable device during infections like COVID-19, i.e., IL-6, IL-8, IL-10, TNF-α [55] or during circadian rhythm, i.e., cortisol; dehydroepiandrosterone (DHEA), and neuropeptide

Y (NPY) [56, 57]. Again, the protein content analysis into sweat must be assessed carefully because the synthesis of analytes such as cytokines may be local. Some reports suggest that the eccrine gland releasing IL-1 and IL-31 serves as an early danger sign, stimulating the keratinocytes, which adopt a proinflammatory behavior [58]. Then, the above may induce a cytokine increase in the sweat that is not occurring in blood. As a general principle, some researchers had concluded that the biomarker partitioning between sweat and blood might be specific according to each biomarker synthesis pattern and transport, i.e., passive, active, or self-generating. Cortisol is an analyte that may be partitioned into the sweat like other small proteins because it exists in two forms into the blood, free and bound to carrier proteins, e.g., corticosteroid-binding globulin [59]. Assuming the last, we discuss several works about cortisol monitoring into the sweat. Nevertheless, it has been hypothesized that a high sweating rate leads to decreased protein sweat content because the large proteins reduce the diffusivity and the membrane permeability [7]. For a comprehensive review of sweat biology, harvesting, and measurement techniques, the reader may refer to recently published works [28, 30, 46]. Additionally, we had recently reviewed the challenges associated with cytokine measurements and the advantages of screen-printed electrodes to measure them [60]. Screen printing is also preferred for fabricating wearable epidermal sensors because this technique allows printing on both rigid and flexible substrates made from cost-affordable and disposable materials.

It is also possible to conclude that sweat composition changes according to the situation [61] and that the best sweat sample comes from the body at rest conditions. Since sedentary sweating ranges from 1 to 5 nL/min per gland [7, 32], a common strategy for sweat sampling is cutaneous pilocarpine nitrate to accelerate sweat production. Although sweat glands release an electrolyte, the holocrine secretion from sebaceous ones lubricates the hair and skin surface with an oily substance that neutralizes the conductive properties conferred by the sweat. Sebum confers a highly electric resistance to the skin (Fig. 1b, c) [9–11]. An iontophoresis process applies a small electrical current cutaneously to surpass the above. The induced electro-repulsion of the positively charged pilocarpine forces its pass from an anode to the sweat glands of the patient [62]. Pilocarpine is a direct-acting parasympathomimetic agent that exerts its action over eccrine sweat glands through muscarinic acetylcholine receptors, inducing sweat production [63]. A study carried out in 2017 demonstrated the reliability of pilocarpine iontophoresis to establish the levels of analytes at blood and its correlation with sweat, compared with the obtained after exercise [64]. The impressive success of the noninvasive biosensing GlucoWatch (Cygnus) system is because it relies on reverse iontophoresis. Since the cells membrane is negatively charged, the commented device cycles a ~0.5 mA cm^{-2} DC between two gel swabs on the skin [65]. Abundant Na^+ ions into the ISF (~ 140 mM) are moved electrophoretically to the cathode, while anions are electrorepulsed, e.g., Cl^-, ascorbate, urate [65]. Cations present at sweat ducts and hair follicles pass through the paracellular spaces among cells, while neutral molecules like glucose and others get out to the skin surface at a rate proportional to the applied potential, e.g., 15–150 nL of ISF at 0.3 mA by 3 min [65]. Two remarkable works made in Prof. Wang's Lab are examples of wearable ionophoresis-sampler biosensors (Fig. 2). Based on his seminal work called panda-like "glucohol" (glucose plus alcohol) tattoo (Fig. 2a–d) [66], a device was recently published for simultaneous monitoring of blood pressure and heart rate with ultrasonic transducers (Fig. 2e–h) [67]. At the same time, electrochemical sensors were coupled to measure glucose, lactate, caffeine, and alcohol (Fig. 2e).

Sonophoresis is another method that uses 20 kHz ultrasound to open micropores and increase the permittivity of the skin, followed by the ISF extraction and its further electrochemical monitoring [68]. Several methods have been recently reviewed for sweat sampling onto wearable biosensors [69].

Here, it is crucial to be aware of the irritation possibility of iontophoretic devices after repeated procedures. GlucoWatch system selling must be stopped in 2007 because it induced skin irritation when used continuously [70]. So, as mentioned above, small proteins like cytokines increase, showing a local effect instead of a systemic one. Additionally, more studies are needed to verify if the iontophoresis process may induce a differential protein blood-to-sweat partition given the promoted electrophoretic movement as a function of the charge and size of the studied protein. Biosensors from Prof. Wang's lab and others have shown sweat sampling autonomously using significantly lesser current and exposition times for iontophoresis that may be 1 mA [71], or even 0.2 and 0.6 mA for 5 min [72, 73]. Here, short periodic sweat sampling may also diminish the harmful risk, then hydrogels with 10% (wt/vol) acetylcholine had been presented a high sweat-rate response (e.g., 354 nL/min/cm^2) for short-lived effect [71]. Then, the commented above WEB devices are safer than GlucoWatch-like devices [74]. In addition, evidence from metabolomics analysis suggests the iontophoresis usability as a harvesting procedure [31].

There are other aspects to be mindful of. Since WEBs expect to interface with the skin, their biocompatibility is pivotal to avoid hypersensibility reactions or contamination from epidermal components. For example, devices that function as continuous films block the regular exchange of sweat by evaporation, leading to trapping it

under for several days. In the end, the uppermost epidermal layer, i.e., cornified, which has sponge properties, will soak and hold the water and solutes, leading to overhydration and maceration of epidermis that may release the excess of analytes to the sweat or even alter the barrier function of the skin [8]. Some efforts to improve the gas permeability and the normal sweat evaporation after sensing had been made. For example, a report used electrospinning polyvinyl alcohol (PVA) to fabricate 300–500 nm fibers that further intertwined in a mesh-like sheet, followed by deposition of a 70–100 nm-thick Au layer on top. After the electrodes were directly laminated on the skin, sprayed water dissolved the PVA, and the nanomesh conductor was attached. Properties of either electrode, e.g., conductivity or skin, e.g., no local inflammation, were stable by a week [75].

Wearable epidermal biosensors (WEBs) design and mode of function for sweat's analysis

According to the transduction mechanism, biosensors that may be integrated onto the epidermis could be mechanical (e.g., temperature, acceleration), electrical (e.g., electroencephalogram), optical (e.g., skin reflected light), or chemical (e.g., protein biomarkers) [49, 78]. Specifically, chemical WEBs for medical purposes usually include dry electrodes that do not require gel before implantation but must be made in a soft-electronic format to avoid the noise from motion, i.e., highly bendable, stretchable, and twistable.

It is possible to identify two basic elements for any WEB architecture, the delivery system for sampling and the analysis region, considering its *modus operandi*. According to the device electrochemical measurement, the analysis region requires at least two electrodes and a contacting sample solution. However, high-performance sensors often add a third reference electrode that helps stabilize the sensor system over time (avoid sensor drift) and therefore help limit the changes in the transduced signal to be only from the specific analyte. A similar tripartite arrangement for WEBs' electrodes is applied in either transistor (e.g., field-effect transistors, FETs) or electrochemical cells (e.g., screen-printed electrodes, SPEs) (Fig. 3a, g): i) point for control of the electrochemical energy (i.e., G in FETs or RE in SPEs), ii) point for energy inlet (i.e., S in FETs or WE in SPEs) and iii) point for energy outlet (i.e., D in FETs or CE in SPEs) [79–81]. Of course, the three quoted categories are relative to the measurement format and associated carriers' charge movement, in such a way that most of them for sweat monitoring have a coplanar disposition concerning the control/inlet/outlet electrodes. The net electron transference occurs between inlet and outlet points, while the density and polarity of charge carriers are regulated by a third control point [76, 77]. Thus, any displacement from a given basal current or potential during charges transference may be registered. SPEs are based chiefly on heterogeneous electrons transfer (hET). In this context, the most used interrogation techniques are amperometry, potentiometry, conductometry, and EIS (Fig. 3c–e) [6]. The advantages and limitations for applying each stated electrochemical technique into the WEBs based on SPEs were reviewed by Bariya et al. FETs do not consider hET, but changes in either voltage or current between G, S, and D are evaluated as detailed below. The fundamental issue is that any thin membrane or material sheet with a surface capable of generating a potential may be used for biosensing onto the epidermis. At the same time, the flow of the carrier's charge occurs depending on the platform type and the electrochemical technique [74, 82–84].

Since human tissue surfaces such as cornea, skin, or mucosa are non-planar, the wearable biosensors must be highly stretchable and very thin to conserve their capacity to complete on-site signal transduction once the biorecognition event occurs. To guarantee its noninvasive patchability and discreetness, WEBs use three strategies at least: i) epidermal or tattoo-like, ii) hard-soft, and iii) functional substrates [84, 85]. Since the electrode's material is lesser lithe, its design requires irregular shapes, e.g., serpentine, mesh, fractal (Fig. 4a) [85–87]. Most wearable formats for epidermal sensing are fabricated over a thermal stable and highly stretchable dielectric substrate like modified polyester (BASF, Ludwigshafen, Germany) [88], silicone elastomer Ecoflex [89], glass fiber-based paper [90, 91], polydimethylsiloxane (PMDS) [92], thermoplastic polyurethane (TPU)/carbon nanotubes (CNTs) composites [93, 94] or even silk fabric-derived nitrogen (N)—intrinsically doped carbon textile (SilkNCT) [95]. The commented material shows Young's modulus (elasticity) near or compatible with the skin (e.g., ~ 60 kPa BASF, 125 kPa Ecoflex, ~ 3 MPa PMDS) [88, 90–95].

Substrates in close contact with the skin prevent any electric interference with the electrodes. The substrate also improves electrical safety, avoids skin irritation, and facilitates the cleaning for reuse or exchange [84]. Since substrate behaves as an insulator, it is described by a capacitor (C_i) and a resistor (R_i) working in parallel (Fig. 1b) [10]. The sensing region (studied below) is coupled to a transducer that converts the biorecognition event into an electrical signal. An amplifier circuit communicates the transduced signal to a pre-programmed microcontroller to calibrate the readout into the linear detection range. The current-to-frequency conversion (CFC) principle is used to process the signal by an analog to digital converter (ADC) [97] into the encoder (i.e., microcontroller) [98]. Finally, the information is sent to a decoder that processes it to be displayed on a user device

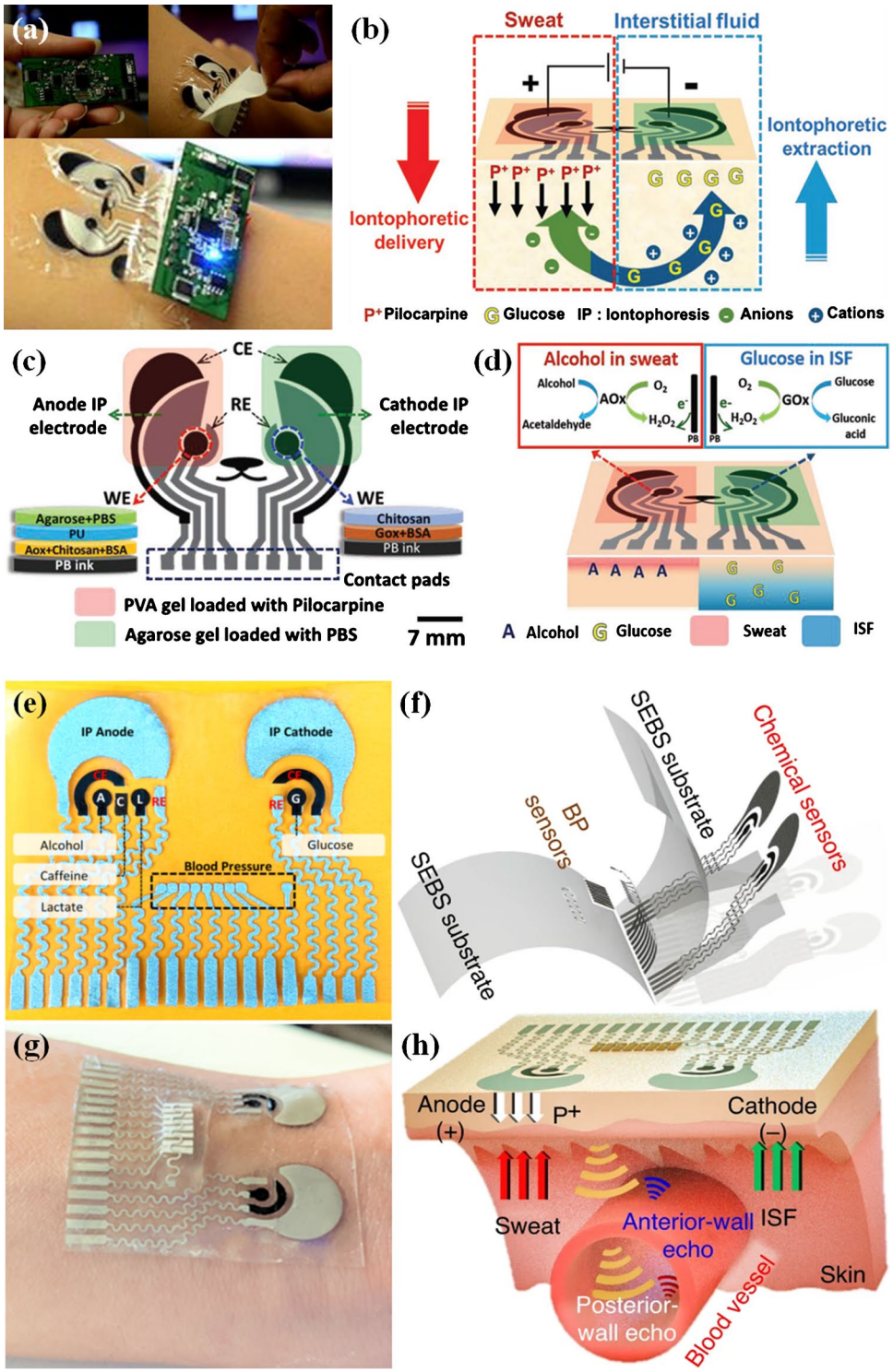

Fig. 2 Panda-like glucohol tattoo (a) releases pilocarpine iontophoretically into the skin to obtain the sweat, while reverse iontophoresis extracts interstitial fluid in a separate location of the rest user (b). A flexible printed circuit board (PCB) is magnetically attached to the electrochemical biosensors, which have been modified with glucose oxidase (GOx) onto the cathode and alcohol oxidase (AOx) over the anode (c). Thus, this wearable epidermal platform analyzes glucose and alcohol in the two biofluids simultaneously and in real-time (d). WE and CE were made with Prussian blue ink while RE with Ag/AgCl ink over a papilio temporary transfer paper-based tattoo (HPS LLC, Rhome, TX). Similarly, a multiplexed device with an additional WE made of carbon modified with multi-walled carbon nanotubes for caffeine assessment is joined to blood pressure (BP) and heart rate ultrasonic sensors (e) through styrene-ethylene-butylene-styrene block copolymer (SEBS)-based stretchable wafer (f). It may be incorporated over the skin (g) to measure hemodynamic and other metabolic biomarkers (h). The disposable screen-printed device is single used on-demand. Reprinted with permission from [66] and [67] respectively

screen. Assembly of all components commented above into a stretchable and twistable ~ 30 µm "skin-like" membrane tattoo was achieved for the first time in 2011 (Fig. 4) [88, 96].

Ideally, the encoder–decoder sending is wireless through a less consuming energy-like Bluetooth Low Energy (BLE) system instead of a radio. Integrated technologies for storage, e.g., flexible batteries, supercapacitors, or harvesting energy, have been proven like autonomous powering sources for self-sensor functioning. While harvesters from light, thermal and mechanical energy have demonstrated high performance, interestingly, sweat may also be used for [99]. A self-powered patch-like simple device made with glass fiber-based paper and enclosed with PDMS has been reported for cystic fibrosis (CF) screening (Fig. 5a, b) [90].

It remained quiescent until the sweat absorption activated a sweat-based battery. When samples with ≥ 60 mM equivalents Cl^- were applied, a threshold voltage value (1.2 V) was reached into a gate electrode of the metal–oxide–silicon FET (i.e., MOSFET; 1.51 V, CF patient). While glass fiber-based paper did not undergo substantial swelling after absorption, it maintained constant the geometry of the electrolyte in a comfortable platform. Other wearable harvesters utilize the sweat redox-active metabolites as mediators to couple a catalytic activity with hET. Immobilized lactate oxidase (LOx) onto an anode is the seminal example in which the perspired sweat provides the substrate, i.e., lactate that feeds an electrochemical reaction, which in turn yields a stable current that may be continuously harvested for the function

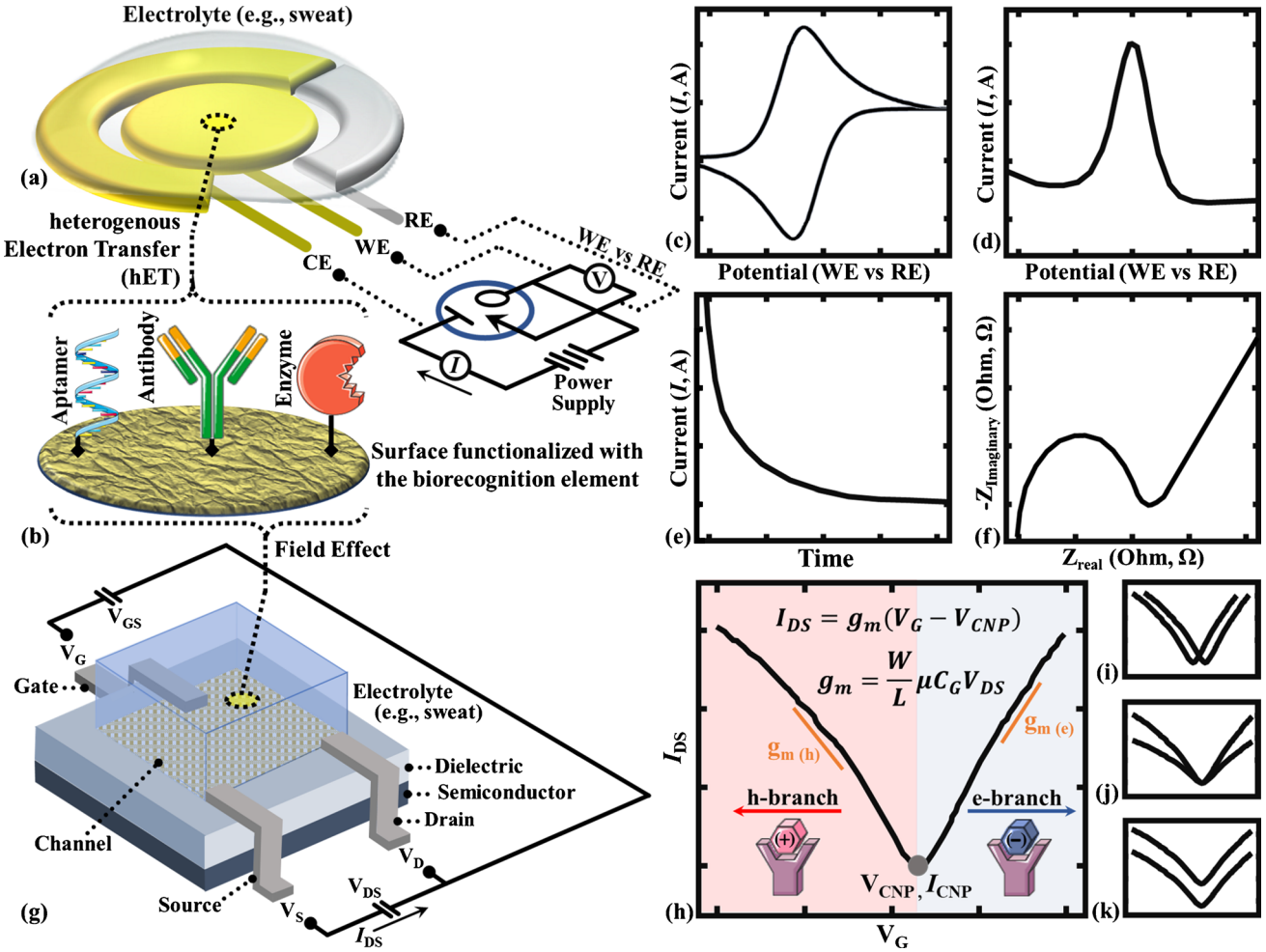

Fig. 3 Similar coplanar tripartite arrangement of wearable epidermal biosensors (WEBs) is applied in either electrochemical cells (a, c–f) or field-effect transistors (FETs); G-K). Commonly the screen-printed electrodes (SPEs) are used for WEBs (a), requiring reference (RE), working (WE), and counter (CE) electrodes. The assembly of a WEB implies the surface functionalization with a biorecognition element or receptor onto (b). Then the interaction with the analyte alters the electron transfer between the heterogenous electrolyte–electrode interface mediated by a redox reaction that is recorded. The applied potential (V) comes from a potentiostat, i.e., power supply, being tuned between RE and WE. Commonly, the current (*I*) is recorded by cyclic voltammetry (c) and differential pulse voltammetry (d). Chronoamperometry is done at fixed potential for rapid measurements (e). Finally, electrochemical cells also can operate under a capacitive approach through the electrochemical impedance spectroscopy (EIS) (f). The detection region of FETs (g), is comprised by the source (S), drain (D) and gate (G) electrodes connected by a channel made of a semiconductor. Here, the current between S and D (I_{DS}) depends from ligand (analyte)-receptor union and normally is considered as a function of the tailor applied D vs S voltage (V_{DS}). If a positive-charged target is held, it will attract negative carriers (i.e., n-doping) and will lead to apart holes displacing the ambipolar V-shaped transfer curve (h) to the right, as well as the associated charge neutrality point (CNP). The last is also true in the inverse sense. The linear behavior from CNP may be described by the shown linear equation, with the transconductance (g_m) as the slope, where the pivotal variables are the width and length of the channel material, the mobility of charge carriers (μ) and the gate capacitance (C_g). Frequently in FETs, the bonding of the analyte to the biorecognition element is done as a record in the I_{CNP} or V_{CNP} changes (i), transconductance at the h- or e-branches (j), as well as differences in the current amplitude of both branch and I_{CNP} (k). Images G–K are inspired from the references [20, 76, 77]. Some images were taken and modified from free smart server medical art

of the device (Fig. 5c–f). Developed electronic skin energy supplies have been reviewed recently by García et al. [100].

Wearable epidermal biosensors based on screen-printed electrodes (WEB-SPEs)

For protein monitoring through wearable SPEs, the WE is functionalized with a bioreceptor to improve the WEB's specificity (Fig. 3b). The arrival of sweat through the delivery region until the sensing region leads to the analyte biorecognition. Since sweat is an electrolyte, a given current (*I*) flows across WE and CE when a customized WE vs RE potential is applied. Finally, the ligand–receptor event alters the hET onto the WE to be monitored. The architecture simplicity of the SPEs explains their scalability in the fabrication process, but on the other hand, the SPE relied devices also show a wide range of analysis possibilities using several electrochemical techniques (Fig. 3c–f). A carefully detailed review of the design and functioning of SPEs for cytokine-like proteins at the point-of-care approach was recently done by us [60]. Prof. Prasad's lab has several examples of WEBs-SPEs (Table 1). The basic prototype of most devices is based on a metalized layer of electrodes, e.g., ZnO, Au, Ag (Fig. 6a) printed over a porous harvester material which in turn is stacked with a watch-like appliance that contains the electronic reader (Fig. 6b, c) [101]. For cortisol sensing through non-faradaic EIS, a two- or three-electrode cell architecture is coupled with an arrangement of hybrid micro and nanoporous layers (Fig. 6d–f). The sweat harvesting using nanoporous membranes improves the performance of electrochemical biosensing because of the macromolecular crowding, nanoconfinement, and filtering by size-based exclusion (Fig. 6g) [102]. The basal-produced sweat at the eccrine and apocrine glands is passively transported to the detection region without the need of neither accumulating sweat nor another iontophoretic-like active methodology for sweat sampling [103, 104]. The applied small sinusoidal AC voltage induces a given capacitance over the WE that generates an output in the form of a phase-shifted current, recorded as a change in the impedance modulus (Zmod) (Table 1). While aptamers as biorecognition elements are smaller than antibodies, they provide greater capacitance given the reached stacking after immobilization. Thus, aptasensor yields a more comprehensive output signal range (30 k − 5 kΩ) [104] compared with a previously reported cortisol wearable immunosensor (10 k − 5 kΩ) (Fig. 6i) [103]. In the end, the final electrode arrangement may be incorporated into the hardware of the previously reported watch-like system called "CortiWatch" (Fig. 6b) [105]. Several changes, covalent coupling of protein followed by loading of the capture antibody in an oriented manner, as well as the incorporation of a platform for determination of the DHEA circadian hormone, allows the researcher to propose and test a robust system termed sensor for circadian clock (SLOCK) [106, 107]. Briefly, the circadian hormones were monitored in the passively produced sweat using EIS and chronoamperometry-relied WEBs. Four hours of testing were considered at three different situations: rest (hours 1 and 2), exercise mediated spike (hour 3), and post-exercise resting (hour 4). Consistently, either cortisol or DHEA increased after exercise, suggesting the reliability of the SLOCK system to avoid background associated with variables like motion, heat, and receptor degradation [107]. WEB-SPE technology for hormone sweat monitoring that controls the circadian rhythm was reviewed recently [57]. The enlargement of the scope analysis of the SLOCK platform for cytokines present at eccrine secretion was made recently by Prof Prasad's lab researchers. An LDR of 50–1000 pg·mL^{-1} for IL-31 [108] suggests the real possibility of ILs monitoring into the sweat by WEB-SPEs. The outstanding device called EnLiSense's skin-SWEATSENSER is capable of sensing four different inflammatory cytokines (i.e., IL-6, IL-8, IL-10, TNF-α) from passive eccrine sweat in a continuous real-time manner (Fig. 6c, h) (Table 1) [55]. The device showed a good correlation compared with ELISA and RIA referent tests in a cohort of 26 subjects (Pearson's $r > 0.98$) but also the ability to distinguish healthy and infected individuals relied on recorded cytokines levels at sweat. Notably, the sweat-to-serum ratio of IL-8 was ~ 1.01 into the rage 2–15 pg mL^{-1} from nine volunteers and a patient cohort of five subjects showing a good correlation between sweat and circulating levels of several cytokines.

The plasticity of SWEATSENSER is because it uses a replaceable strip with the same electronic reader (Fig. 6c). Thus, the strip may be functionalized with other bioreceptors during the sensor fabrication process and then adapted for. To illustrate, the detection of IL-1β and C reactive protein (CRP) in the sweat using SWEATSENSER technology variates only in the use of monoclonal IL-1β or CRP capture antibodies to trip functionalization (Table 1), which also reports a Pearson correlation of $r > 0.90$ either IL-1β or CRP, in comparison with ELISA [109].

Finally, NPY monitoring by WEB-SPEs had been recently achieved also by Prof. Prasad's lab. A non-porous concentric pattern of gold WE/RE interdigitated electrodes arrangement (135 mm^2 area) was compared with a three-electrode interdigitated platform. The former design minimized the field interferences from edges while the latter increased the overall capacitance of the system and can operate with ultra-low volumes of sweat (Table 1) [102]. The use of (non-) faradaic EIS and chronoamperometry confirmed the platform's usability to measure NPY in concept tests even at 10 pg/m. NPY is a 36-amino acid polypeptide that, despite its expression throughout the central and peripheral nervous systems, has been associated with several microenvironments as the inflammatory one [117]. Immune cells

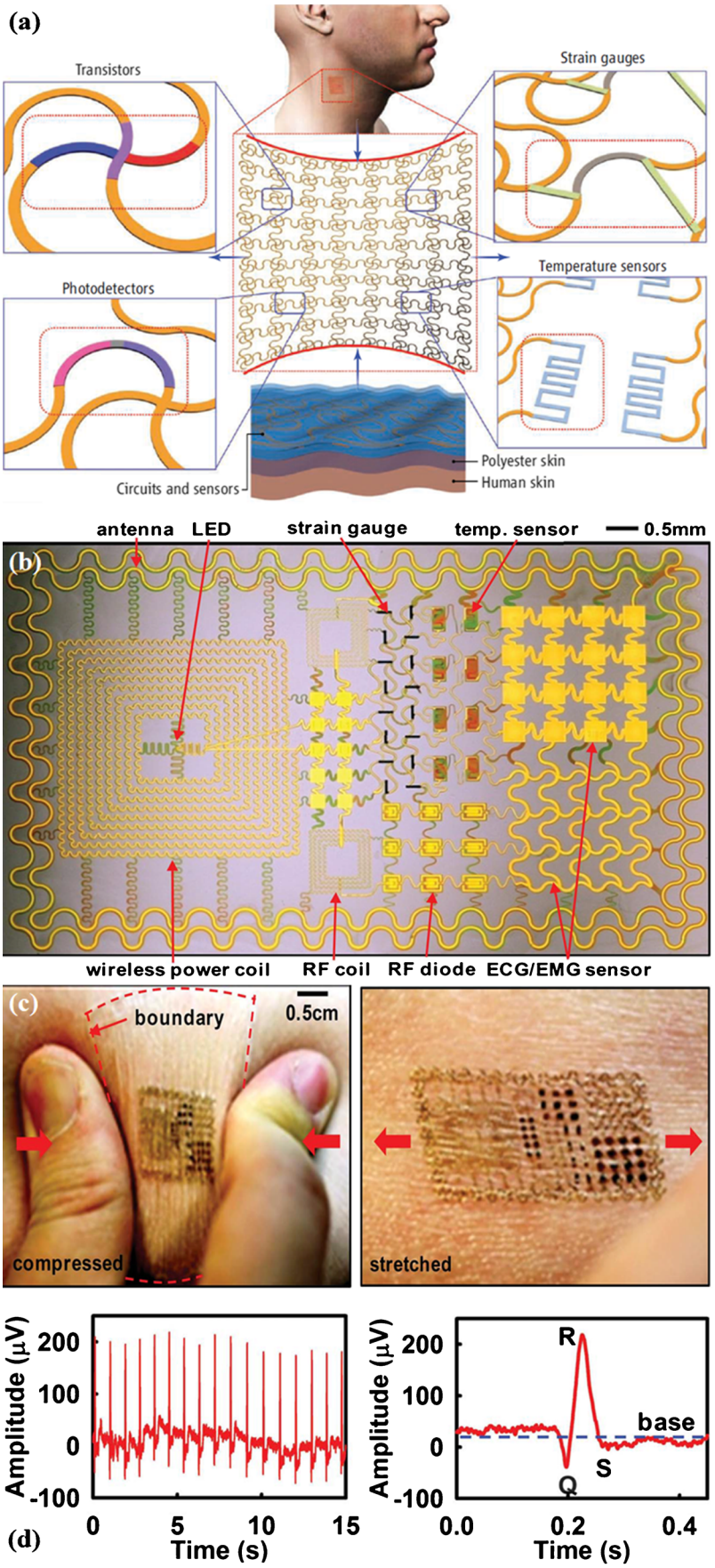

Fig. 4 Bandage tape-like format device showing the irregular form of electrodes to ensure flexibility and avoid the motion noise (a). Peeled off natural skin engineered to be attached through van der Waals forces. Multifunctional integrated electronic details are shown (b). Despite mechanical stress (c), it may assess the temperature and carry out either an electrocardiogram (ECG) (d, whole heart pulsation on the left; single heartbeat magnification on the right) or electromyography (EMG, not shown). Note that components such as wireless, radio frequency (RF) and antenna are shown. Reprinted with permission from [88, 96]

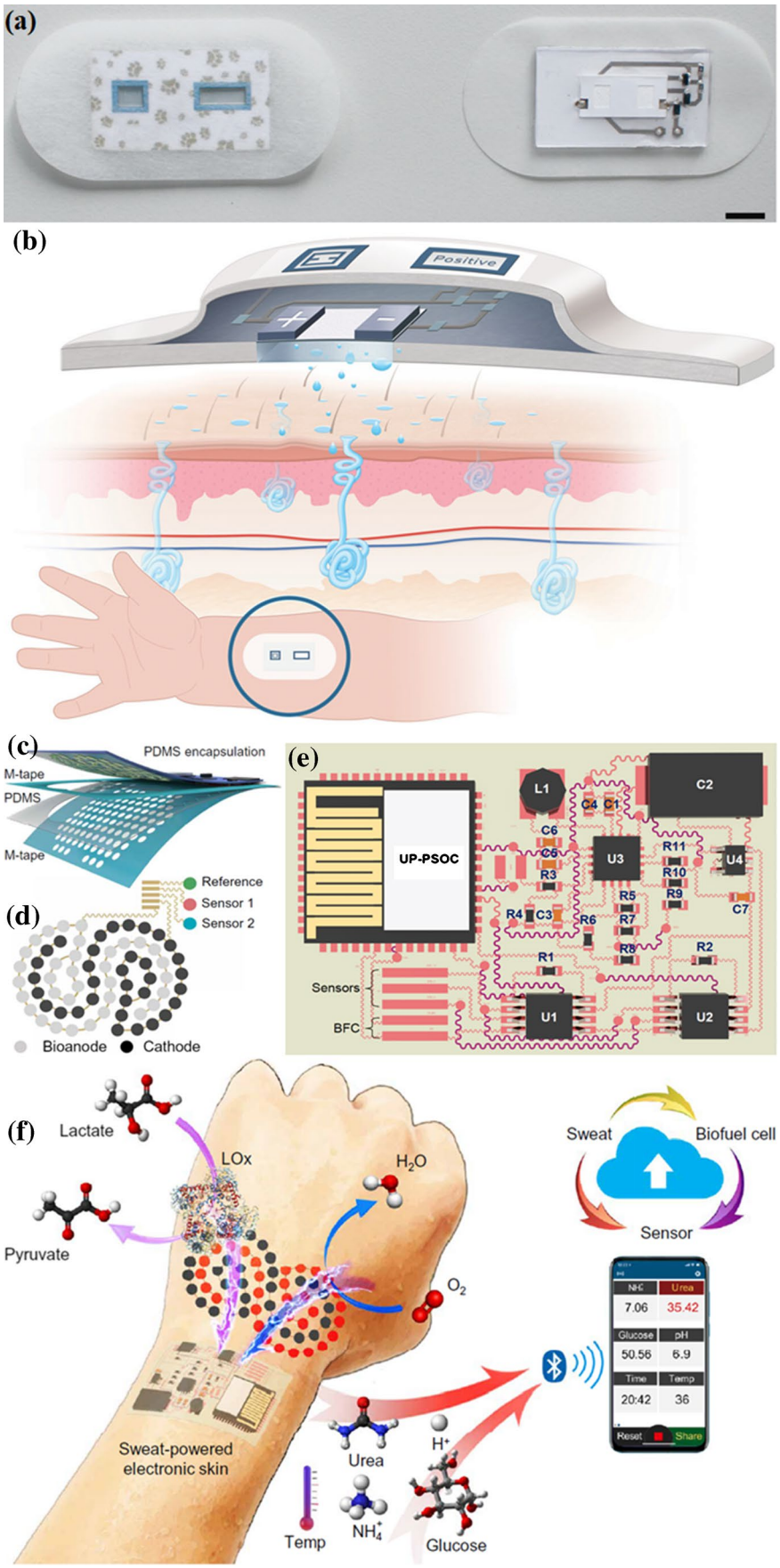

Fig. 5 The basic design of a "battery sensor," where the sensor and battery are merged in a single element (a). After sweat absorption, the Mg-anode and AgCl-cathode are connected by a hydrophilic glass fiber-based paper, leading to: $Mg_{(S)} + 2AgCl_{(S)} \rightarrow Mg^{2+}{}_{(aq)} + 2Cl^-{}_{(aq)} + 2Ag_{(S)}$ ($E° = 2.59$ V). If the sweat conductivity exceeds 60 mM equivalent NaCl, an electrochromic display is turned on as "Positive" (b). In another approach, biofueled cells are enclosed into PMDS (c). A microstructured Au bioanode (d) with a large electroactive area is modified with lactate oxidase to transform lactic acid into pyruvate. Pt alloy nanoparticle-decorated cathode mediates oxygen reduction to water, charging the harvester power (U3, BQ25504) of the soft electronic–skin interface (e, f). Once the analyte is monitored, a Bluetooth Low Energy (BLE, UP-PSOC) system wirelessly transmits the information to the user interface. Reprinted with permission from [90] and [89], respectively

such as macrophages express NPY receptors that have been associated with immune regulation. Thus, the correlation between the observed proinflammatory profile and the high levels of NYP in people with major depressive disorder (MDD) was investigated actively. A study demonstrated the correlation between premenopausal women with MDD in remission and the high levels of NPY into the sweat, which may help follow and predict the complications like cardiovascular disease, osteoporosis, and diabetes [118]. WEBs may improve these approaches because continuous real-time monitoring may track disorders like chronic anxiety and MDD via self-monitoring of NPY.

Wearable epidermal biosensors based on field-effect transistors (WEB-FETs)

FETs are solid-state electrodes that commonly operate by a tunable 2–30 V. These kinds of transistors have efficient electrical power consumption, emit negligible heat, and, as any transistor, may self-amplify the electrical signals [81, 87, 119]. WEBs based on FETs have a basic architecture that contains a tripartite terminal system (i.e., G, S & D) and a semiconductor channel that serves as a bridge for electric flow between S and D (Fig. 3g). Impure or intrinsic semiconductors are mainly used as a channel. When the used semiconductor is doped with trivalent elements, e.g., boron, gallium, the channel is rich in positive valences or holes, i.e., p- or acceptor-type, but the doping with pentavalent elements, e.g., arsenic, antimony increases the negative charges or electrons, i.e., n- or donor-type. Most channels for health monitoring are separated from G electrodes by a dielectric layer over [23] to improve the internal structure of the semiconductor and to ensure a uniform penetration of applied voltage [120, 121], e.g., metal–oxide–silicon in the case of MOSFET and electrical-double layer in the case of ion-sensitive FETs (ISFETs) [20, 79, 80]. While WEB-FETs for sweat analysis are commonly liquid-gated [122], ISFET-like are the most used, which may detect ions as H^+, Na^+, K^+, or Cl^-. Graphene (GFET) or an organic π-electron system (OFET) is immersed into the electrolyte sample, together with a reference electrode forming a gate-like structure because the EDL formed onto functions as a dielectric. The G electrode is also made from a semiconductor material and is coupled to a circuit that introduces a customized electric field through an insulating layer, i.e., G-S voltage, V_{GS}. The flow intensity of the charges between D and S, i.e., D–S current, I_{DS} is tuned by the applied V_{GS} over the channel material, controlling it. Compared with conductors, semiconductors have a lower charge density, i.e., electrons and holes, enabling the applied potential to penetrate quite far into, despite its relatively weak power, and modifying the conductive properties of the surface material or, what is the same, displacing the charge of the transistor's conduction channel.

A biorecognition element is immobilized, e.g., antibody, aptamer, enzyme at the surface to associate their changes on electric properties during the interaction with a specific analyte. Since the microenvironment of conductive material determines the features of the channel, any change at its surface alters the charge passing density, i.e., the current and the associated readout electrical metrics, a phenomenon termed field effect, which affects just the more near surfaces, decreasing rapidly with distance [77]. The last is particularly true for vdW materials like graphene and other low-dimensional structures such as nanowires and nanoribbons because their surface-to-volume ratio enhances the sensitivity and allows a very low limit of detection (LOD) [123, 124]. As proof, increasing V_{GS} decreases channel resistance to establish a significatively I_{DS} because the basal V_{DS} forces the charges to flow through in the S → D direction. Whether G or channel surfaces are coated with a biorecognition element, the voltage (V_G) alteration produced by a given concentration of ions after a given biorecognition event may be assessed as a function of the analyte concentration [125]. Then, the inlet signal I_{GS} is altered, modifying the outlet I_{DS} into the channel, amplified for further readout processing. In brief, if any of the three parameters V_{DS}, I_{DS}, or V_{GS} vary, the other two will fine-tune their behavior either linearly, e.g., any V_{GS} increase leads to a significatively I_{DS} increase or saturated, e.g., I_{DS} is not modified despite any increase in any V_{DS} [79, 81]. In a transfer plot (Fig. 3h), the typical V-shaped D-S current (I_{DS}) signal is obtained when D-S electrodes are continuously biased in a saturation mode while the G voltage (V_G) seeps. Here, the I_{DS} is primarily controlled by the V_{GS} but weakly dependent on V_{DS}, so a density decrease in the positive carriers or holes (i.e., left branch or p-branch) is experienced while electron transfer increases gradually (i.e., right branch or n-branch) (Fig. 3h).

The minimum V_G, where the holes and electron populations are proportional and the minimum of current is registered, is termed charge neutrality point (CNP). A linear behavior may be observed from CNP, also called the Dirac point, because it is described by the linear equation shown in Fig. 3h [20]. It is worthwhile to note that the amplification role of FET is accomplished because the biorecognition event introduces small changes in applied voltage, resulting in significant changes of current, or vice versa (Fig. 3i). Once the potential is established, the electrolyte ions around the semiconductor surface are reoriented based on their charges, leading to EDL near the microenvironment. Since the thinness of commonly used semiconductors onto FETs, e.g., graphene, a very small EDL is also formed at nanometer or even angstroms scale, resulting in a large gate capacitance, which is in turn relatively easy to measure

Table 1 Some representative examples of wearable electrochemical biosensors (WEBs) for protein and hormone measurement in sweat

WEB TYPE	PLATFORM FEATURES	METROLOGY	REFERENCE
Aptasensor (SPE)	**Sample:** Sweat **Analyte:** Cortisol **Electrode:** Silver WE and RE printed onto nanoporous zinc oxide (ZnO), deposited on a hydrophilic polyamide microporous membrane. **T:** 2.5 µm; **Functionalization:** Thiol at the 5′ end of cortisol single stranded DNA aptamer is crosslinked with the ZnO SAM using DTSS **Passivation:** NSB was avoided using microporous substrate **Technique:** Non-faradaic EIS; 100 Hz; with 10 mV AC amplitude	**LDR:** $1-256$ ng mL^{-1} **Time of response:** 5 min **Stability:** > 1 week. Remains active after 8 h of use	[103, 104]
Immunesensor (SPE)	**Sample:** Sweat **Analyte:** Neuropeptide Y (NPY) **Electrode:** Gold interdigitated WE, RE and CE, printed onto nanoporous polyamide substrate **Functionalization:** Thiol binding between anti-NPY and WE using DSP linker **Passivation:** NSB was reduced by the size-based exclusion induced by the nanoporous substrate **Technique:** a) EIS; 1 Hz – 1 MHz; with 10 mV AC amplitude; b) ChA: DC step potential of 600 mV by 60 s	**LDR:** $10-500$ pg mL^{-1} **Time of response:** 1 min **Stability:** Not shown	[102]
Immunesensor (SPE)	**Sample:** Sweat (10 µL) **Analyte:** IL-1β, IL-6, IL-8, IL-10, TNF-α, CRP **Electrode:** Interdigitated RE and WE made of ZnO printed onto nanoporous polyamide substrate **Functionalization:** Monoclonal antibodies cross-linked by DTSSP through thiol-bond **Passivation:** Tween 80 **Technique:** Non-faradaic EIS; 180 Hz, with 10 mV AC amplitude	**LDR:** a) Cytokines: 0.2–200 pg·mL^{-1}; b) CRP: 1–10 ng·mL^{-1} **Time of response:** Immediately **Stability:** > 1 month	[55, 109]
MIP-FET	**Sample:** Sweat **Analyte:** Cortisol **Electrode: S, D & G:** Ag/Cl; **C:** PEDOT:PSS; **B:** SEBS elastomer; **T:** 100 µm; **Functionalization:** MAA as Cortisol-selective polymer and EDMA as cross-linker **Passivation:** Non-required **Technique: i) V_G:** 0.2 V; **ii) Output:** I_{SD}; **iii) Doping polarity:** n	**LDR:** 0.1 – 10 µM **Time of response:** ~ 6 min without microfluidic system; 1 s with it	[110]
BRE-FET	**Sample:** Sweat **Analyte:** Neuropeptide Y (NPY) **Electrode: S & D:** 1/40 nm of Ti/Au; **G:** Ag/Cl; **C:** Graphene; **B:** Silicon; **T:** 285 nm; **Functionalization:** Pi stacked PBASE on channel reacts with N-terminus and at Lys11 of P1N3 BRE **Passivation:** Non-reported **Technique: i) V_{DS}:** 0.1; **ii) Output:** ΔV_{CNP} calculated as the difference of V_{CNP} from each I_{SD} vs. V_{GS}; **iii) Doping polarity:** n	**LDR:** 1 pM – 10 µM **Time of response:** ~ 15 min	[111, 112]

Table 1 (continued)

WEB TYPE	PLATFORM FEATURES	METROLOGY	REFERENCE
Aptasensor (GFET)	**Sample:** Sweat, tears, saliva, serum, urine **Analyte:** IL-6, TNF-α, IFN-γ **Electrode: S, D & G:** ~4/46 nm of Cr/Au; **C:** Graphene; **B:** PEN or biaxially oriented PET (Mylar film); **T:** 2.5 µm **Functionalization:** π-π stacked PASE or Nafion **Passivation:** Tween 80 **Technique: i)** V_g**:** − 0.2 to 0.4 V; **ii)** V_{DS}**:** 0.01 V; **iii) Output:** I_{SD}; **iv) Doping polarity:** n	**LOD:** a) IL-6: 6.11 fM; b) TNF-α: 6.08 fM. c) IFN-γ: 4.76 fM. **Note:** The best values of cited works are shown **Time of response:** 5–7 min	[113–116]

Abbreviations: *B*, body of FET or substrate; *BRE*, biological recognition element; *C*, channel; *ChA*, chronoamperometry; *CRP*, C reactive protein; *D,* drain electrode; *DSP*, dithiobis-[succinimidyl propionate]; *DTSSP*, 3, 3′-dithiobis-(sulfosuccinimidyl propionate); *EDMA*, ethylene glycol methacrylate; *EIS*, electrochemical impedance spectroscopy; *G* gate electrode; *GFET*, graphene field-effect transistor; *L*, large; *LDR*, linear dynamic range; *MAA*, methacrylic acid; *MIP*, molecularly imprinted polymer; *PASE*, 1-pyrenebutanoic acid succinimidyl ester; *PBASE*, 1-pyrenebutyric acid N-hydroxysuccinimide ester; *PEDOT:PSS*, poly(ethylenedioxythiophene): poly(styrenesulfonate); *PEN*, polymer polyethylene naphthalate; *PET*, polyethylene terephthalate; *S*, source electrode; *SAM*, self-assembled monolayer; *SEBS*, styrene-ethylene-butylene-styrene; *SPE*, screen printed electrode; ***T*****,** thickness; V_{CNP}, voltage at charge neutrality point; V_{DS}, drain-source voltage; V_G, gate voltage; *W*, wide; *WEB*, wearable epidermal biosensor.

[129]. The applied gate potentials required to overtake the Dirac point are small (e.g., ± 1 V). Registered I_{DS} vs. V_G signal is affected by the semiconductor doping state so that the CNP for intrinsic ones is reached at 0 V_G. The modifications at the semiconductor surface explain the observed V-shaped behavior, where the left part corresponds to high positive carriers or holes density, i.e., p-doping, while the right appears if the electron flow is meaningfully more significant than the holes, i.e., n-doping. Similarly, the electrostatic gated effect predicts that if the recognition elements capture a positive-charged target, it will tend to attract negative carriers, i.e., electron trapping, leading to an n-doping, and vice versa (Fig. 3h) [111, 119].

Inconsistencies observed from the expected behavior have been associated with degradation, altering target structure or impurities into the measurement system. The pH is crucial during protein determinations because any variation can alter the deprotonation state of its amino acid groups, leading to unexpected behaviors of p- or n-doped branches in the transfer curves. For instance, Kim et al. reported an immunosensor based on reduced graphene oxide-FET, which was n-doped at pH 7.4 when the studied analyte (i.e., prostate-specific antigen/a1-antichymotrypsin; PSA-ACT) was negatively charged but underwent a p-doping when the analyte was charged positively at pH 6.2, under its isoelectric point (i.e., pI 6.8) [130].

Apart from CNP changes, a different measurement approach may be made when transconductance (g_m) variations are recorded (Fig. 3j) [131]. This parameter results from the ratio between current change at the output port and the voltage change at the input port. In terms of FETs, the g_m is defined by the ratio of the small changes in the D current (δI_D) and the small changes in the G-S voltage (δV_{DS}) with a constant biased D-S (i.e., $g_m = \delta I_D / \delta V_{DS}$). In other words, g_m of any FET corresponds to a performance feature that estimates its proficiency to convert a slight change in voltage in a substantial current readout [76]. Thus, because analyte binding behaves as a new scattering site, it changes the basal charge's velocity flow, i.e., mobility, µ. Slope variations in either p- or n-branches of the transfer curve are further registered (Fig. 3j). Finally, it may be easier to measure the variation in the charges stream through the channel, i.e., electrical current at a fixed VG, but since it depends on both charge's density (n) and velocity (v), it is not easy to separate the contribution from either during data processing. The above also explains the associated CNP and g_m (i.e., p-/n- slope) variations (Fig. 3k). Notwithstanding wearable epidermal FETs for protein measurement from sweat are relatively scarce, these devices have shown advances in development, including material improvements and the increased complexity of the evaluated analytes [126–128].

While the platforms shown in Fig. 7 was not designed for protein measurement, it gives an idea about the feasibility of FET-based technology for wearable fabrication with cost-affordable materials. In WEB-FETs for sweat analysis, the sample delivery over the ISFET must be controlled so that the channel and the reference electrode are the unique ones exposed (Fig. 7c–e). To illustrate, the molecularly imprinted polymer (MIP) technology was used by Parlak et al. to synthesize a molecularly selective cortisol-membrane (Fig. 8A, B), which, together with a microfluidic system, controlled the sweat delivery to the sample reservoir and sensor further (Fig. 8c, d). Notably, while molecules like cortisol are neutral, the obstruction of MIP by cortisol alters the flow of ions to the channel, simplifying the measurement format (Fig. 8e) for the flexible device (Fig. 8f, g). Similarly, three works based on aptamers show the reliability of the stretchable GFETs for cytokine measurements in sweat and

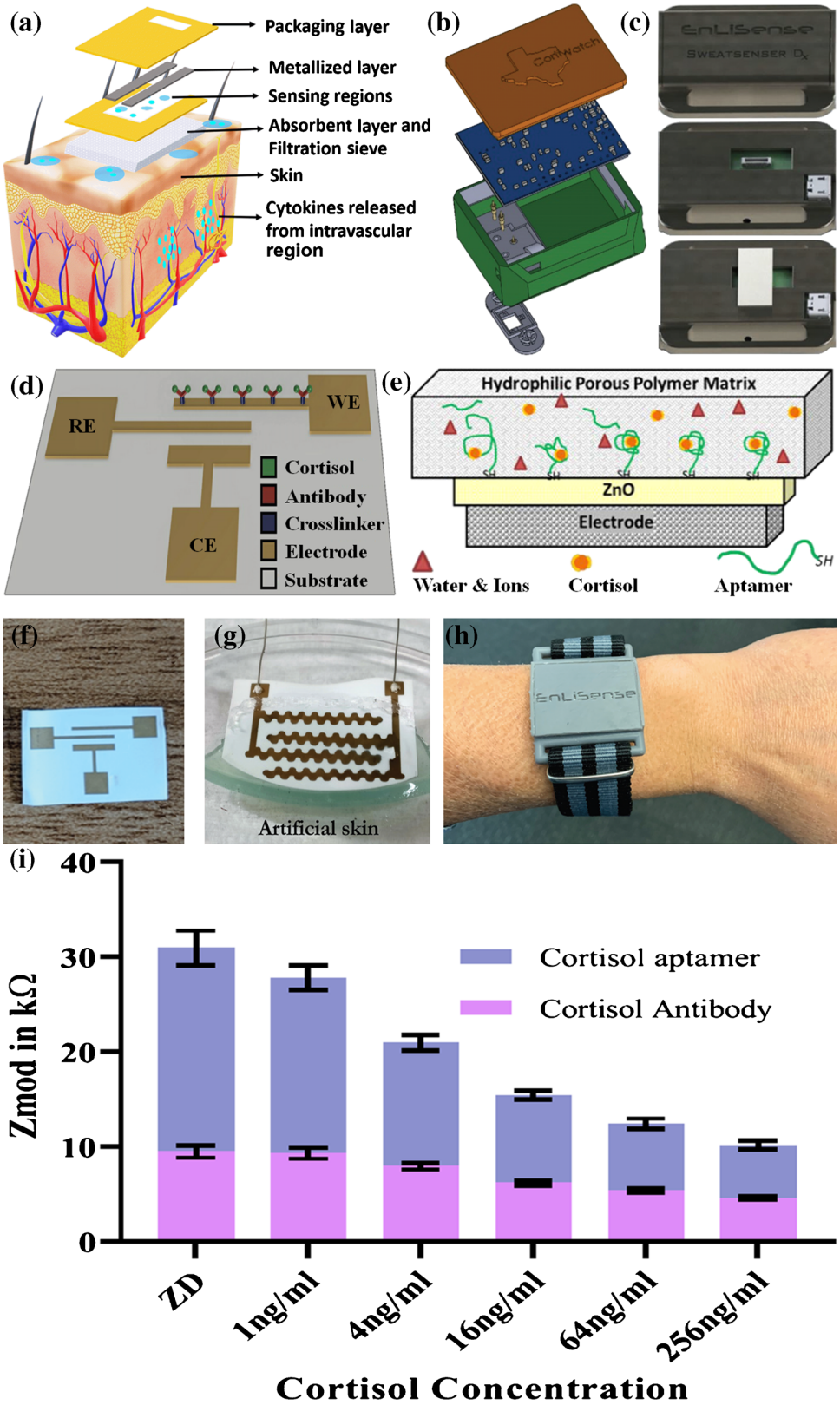

Fig. 6 Wearable epidermal biosensors based on SPEs include a micro- and nano-absorbent layer (a) stacked under the electronic arrangement for wireless sensing (b). The reader (c, top) has a slot (c, middle) for mounting sensor trip (c, bottom). WE may be modified with antibodies (d) or aptamers (e) using three electrodes (f) or two serpentines (g). The synergism between hydrophilicity and porosity of the polyamide membrane (i.e., ~ 200 nm), permits a rapid and uniform percolation (i.e., < 1 min) of the sweat produced at steady-state, for a real-time measurement. ZnO is biocompatible and semiconducting (i.e., band gap 3.367 eV), but also is suitable for thiol-crosslinking. According to the analyte concentration (i.e., cortisol, ILs, NYP, CRP) in the sweat, the aptamer or antibody binding activity modulates the dielectric properties of the EDL formed by the ions and water molecules around the electrode-sweat interphase, which in turn is possible to be sensed by the watch-like wearable device (h). The records using aptamers suggest a greater signal compared with the use of antibodies (i). Reprinted with permission from [55, 104, 105, 109]

other biofluid samples without labels (Fig. 9a–g) [113–116]. The further development of the above had allowed its multiplexing for cytokines storm monitoring during severe acute diseases like COVID-19 (Fig. 9h, i) (i.e., IL-6, TNFα, IFNγ) [132]. The reported device uses the Tween 80 for passivation and a dual channel system to adjust the aptamer–cytokine

binding onto the sensing unit with the background generated onto a reference unit (Fig. 8h) [110]. In the end, the generated data is sent wireless to a connected Android smartphone.

NPY had also been tried to be monitored into the sweat using the WEB-FET system. A recent work uses short 12-mer peptide as biological recognition element (BRE) called PN1 (HSSYWYAFNNKT) (Fig. 10) (Table 1) [111]. Interestingly, the use of liquid cell transmission electron microscopy (LC-TEM) variation enabled researchers to study the interaction of the graphene chemisorbed PN1 and the NYP at the same time of measurements [112]. The last quoted platform was carried out in artificial sweat and was modeled using Gouy–Chapman–Stern representation for liquid-interface interaction. It partially explains the screening effect by direct observation. It recalls the importance of basic research to ameliorate limitations associated with the charge screening, for future WEB-FETs devices, especially for the real-time sensing of small charged biomarkers like NPY [111].

Up to date, reviews have been made either detailing the general requirements for stretchable FETs fabrication [87] or focusing on the advantages conferred by the two-dimensional materials to the wearable electrochemical biosensor devices (e.g., lightweight, biocompatibility) [9–11, 18–133].

Challenges of WEBs design and possible solutions

Based on the advantage that confers decreasing size device in terms of sign-to-noise gaining, the commented designs need to consider the minimal scale and its shape and geometry to confer higher surface-area-to-volume ratio, reduce screening time and offer reliable mass-transport times. Like most body fluids, sweat has a considerable ionic strength that packs the counterion so close, or the same, decreases the Debye length (λ_D) and improves the associated electric screening [129]. Consequently, small Debye lengths into biological samples (e.g., $\lambda_D = 0.7$ nm in 1X PBS) should promote the remotion of the analyte from the G or WE surface [134]. Strategies to reduce the Debye screening in FETs that use a static (direct current, DC) gate bias have been summarized in (i) improving synthesis in channel material to attain distinct morphologies and charges distributions, (ii) redesigning the receptors size smaller than the λ_D, and (iii) increasing the λ_D by electrolyte dilution [13, 77]. It has been suggested that, since electrodes with concave surfaces surround more the electrolytes than either flat or convex, it also highly ameliorates the Debye screening and experiences lesser capacitance, improving the sensitivity [135].

Other analytical approaches suggest that a hemispherical electrode less than 50 nm forms a curved EDL with a large diffuse layer, growing the surrounding ionic cloud thickness [136]. It is associated with a capacitance increase and a drop of the potential from the outer Helmholtz plane, affecting the tunneling length for hET in the case of SPEs. Some promising strategies based on capacitance or associated EDL formation have demonstrated the biosensing feasibility into strength ionic liquids like a serum. Under positive gate bias, a microfluidic coupled device induces the formation of a positive EDL onto a channel made of aluminum gallium nitride (AlGaN) and negative ones onto a gold G electrode, increasing the output drain current. Thus, analyte binding onto G induces a V_G drop leading to a local redistribution of the charge density, altering the charge density on the active channel. The above allows the rapid (i.e., ~ 5 min) and highly repeatable serum measurement of either neutral or charged proteins without washing requirements in significative clinical levels (e.g., C reactive protein, 1 fM–26 nM) [137]. Then, the high sensitivity observed by tunnel FET-based biosensors may be because of its concave arrangement at the cavity [131].

Since most sensors require a minimum analyte threshold at their surface to produce a substantial output, the accumulation is also decisive. Before moving on, it is precise to assume that all the sensing region (i.e., G, channel, or WE) is covered by the bioreceptor since, otherwise, the signal-to-noise ratio decreases while the signal derives to a more significant area than that where the analyte binding takes place [123].

Analytical considerations suggest that, in steady-state, a hemisphere-shaped nanobiosensor surface can accumulate in a time 11% more molecules than a disk of the same area [138]. In terms of WEBs, it means that an extremely small design could require more extended periods to accumulate a given threshold of molecules for positive detection, affecting the time of response for continuous real-time monitoring [139]. Of course, the last is especially true for diluted analytes such as protein biomarkers, making the LOD per unit of time one of the most critical criteria to estimate the wearable biosensor performance. Here, the affinity level of biorecognition elements, joint with the sensibility of the sensor's surface, must be considered to surpass the mass-transport limitations imposed by convection (far away from the sensor) and diffusion (close to the sensor). It, in turn, may be optimized by microfluidic system delivery or electromagnetic concentration strategies [91, 140, 141], especially in the case of sweat where the unidirectional flow does not occur naturally [6]. Since sample volume is not the limiting factor for wearable sensors because it is in close contact, the measurements should be as rapid as electrochemistry enables. For example, a hard/soft composite system used a high-molecular-weight silicone oligomer (Sylgard 184, without curing agent) for appliance fluid immersion, which in turn was enclosed between substrate/superstrate silicone

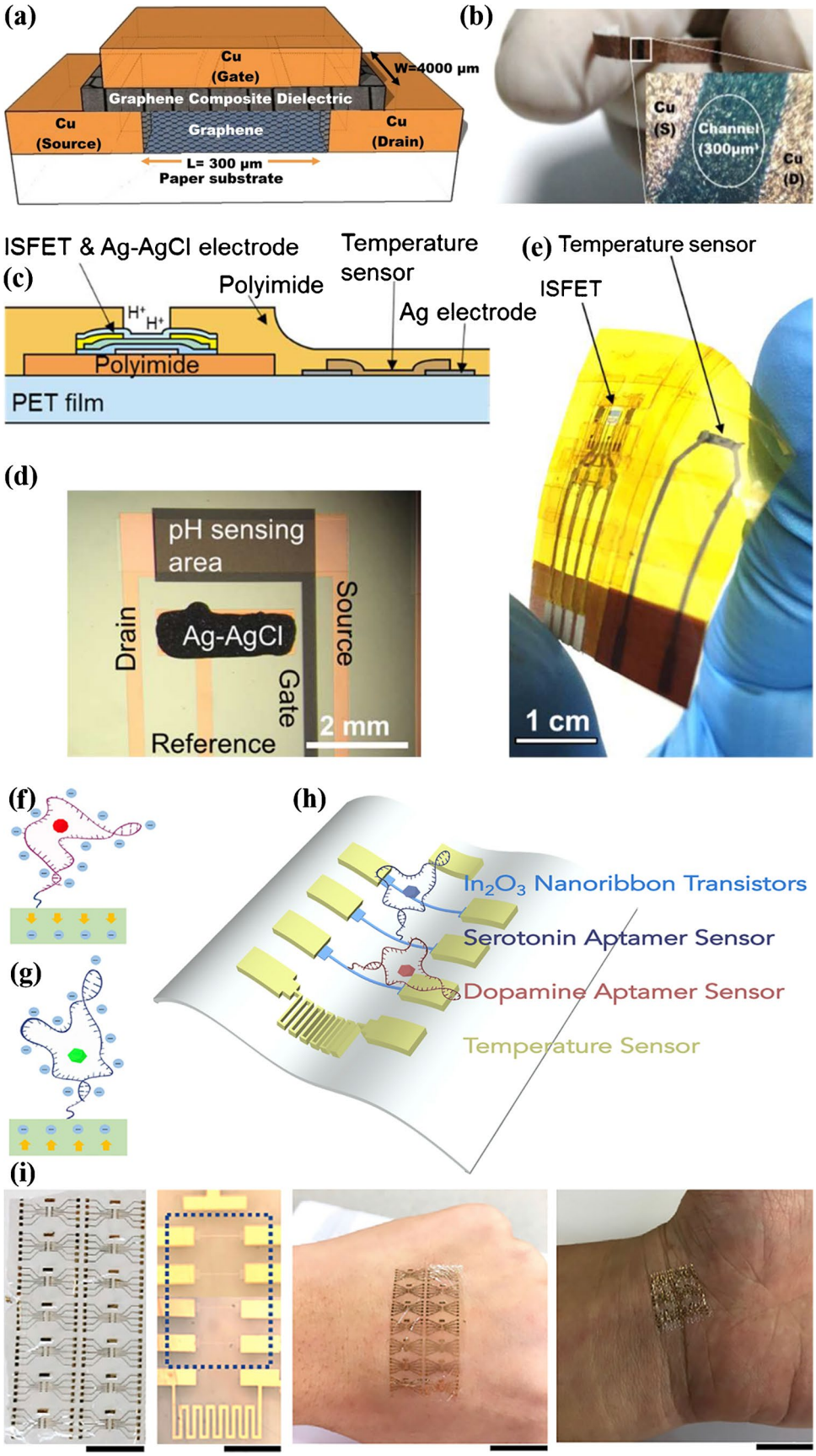

Fig. 7 Important developments in wearable FET-based biosensors. A simple graphene-based FET was made through screen-printing Cu over cellulose paper substrate as S/D/G and graphene/graphene oxide composite as a channel (a, b). Using polyimide-Si wafer substrate, an ISFET printed over Al/Al_2O_3 (G), InGaZnO (Channel) and Au (S/D) (c), to detect H^+ (d), while did sense the temperature through another printed Ag electrode directly over a flexible polyethylene terephthalate (PET) film, cured at 70 °C (e). Multiplexed FET was achieved by the immobilization of aptamers that increase (f) or deplete (g) the channel electrostatically after dopamine (red) or serotonin (green) union. The In_2O_3 nanoribbons were sputtered on a thin PET substrate (1.4 µm) (h). The fabricated array has fourteen devices (i, left, 1 cm bar) with four nanoribbon-FETs by each one (i, middle-left, dotted blue box, 500 µm bar). Gold was used for the common-gate electrode and the resistive temperature sensor (from top to bottom). The obtained device was stretchable and wrinkable (i, middle-right and right, 2 cm bar). Reprinted with permission from (a, b) [126], (c–e) [127] and (f-i) [128]

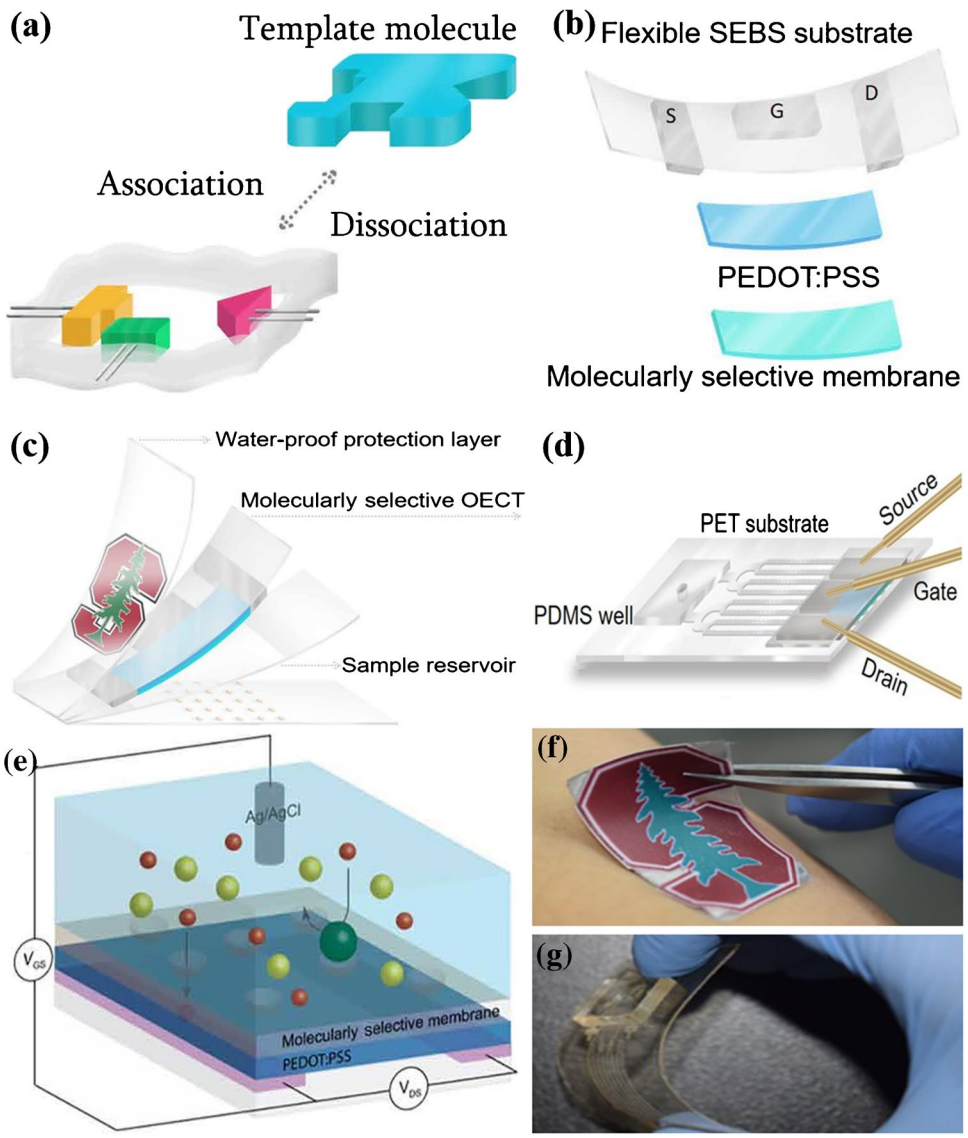

Fig. 8 The cortisol was used as a template molecule for a molecularly imprinted polymer with selective properties (a). The above was stacked over an organic channel made from poly (ethylenedioxythiophene): poly (styrenesulfonate) (PEDOT: PSS), and over the Ag/AgCl FET, which was brush-printed onto a styrene–ethylene–butylene–styrene (SEBS) elastomer substrate (b). A microcapillary channel array conducts the sweat to the sample reservoir and the organic electrochemical transistor (OECT) (c). When a microfluidic device was used, the sweat sample was immediately delivered over the sensor (d). The ΔI_{SD} was strongly reduced when cortisol was present because the membrane pores become sealed, blocking the ion flow to the channel (e). Finally, both sensing (f) and microfluidic device (g) maintained essential flexibility. Reprinted with permission from [110]

elastomers (Ecoflex, Smooth-On, Easton, Pennsylvania) (Fig. 11). Although the above was not used for protein biomarkers assessment, and the microfluidic suspensions were used for mechanic isolation, this type of device suggests plausible ways to introduce microfluidics into the WEBs as sampling delivery systems. Briefly, the sensor's geometry affects the time needed to produce a steady-state signal, only achieved when the union between the analyte, into the sample, and the biorecognition element, onto the biosensor, be at equilibrium [139]. To illustrate, while planar FET and WE may interact with the sample just in one of its sides (1D), nanostructures like nanowires (2D) and nanospheres (3D) include the perpendicular interaction, accomplishing the equilibrium faster, and its associated steady-state signal [125]. Thus, nanostructured devices may help overcome the required response time to detect an analyte in a real-time manner.

Miniaturization has been proposed to make less invasive strategies. Since conventional flat-electrode includes only 1D sample flow and is lesser flexible, nanopatterned electrodes like porous surfaces, nanomeshes, and atomic phase structures have been developed [86]. Microneedle-based platforms are applied in a pseudo-invasive manner. In electrophysiological monitoring, microneedles minimize the insulating effect of the more external stratum corneum because the body of the needles surpass this skin layer and put in direct contact with the other more conductive epidermal layers (i.e., granular, spinous, and basal). The simplified electrical equivalent circuit showing the electrode coupling and the conductive epidermal layers are shown in Fig. 1c [10]. For chemical WEBs, four epidermal layers must be crossed over to sample the dermis. A microneedle two electrodes array (i.e., Cr/Pt WE, Ag/AgCl RE) was implanted transdermally onto human skin for enzyme-based

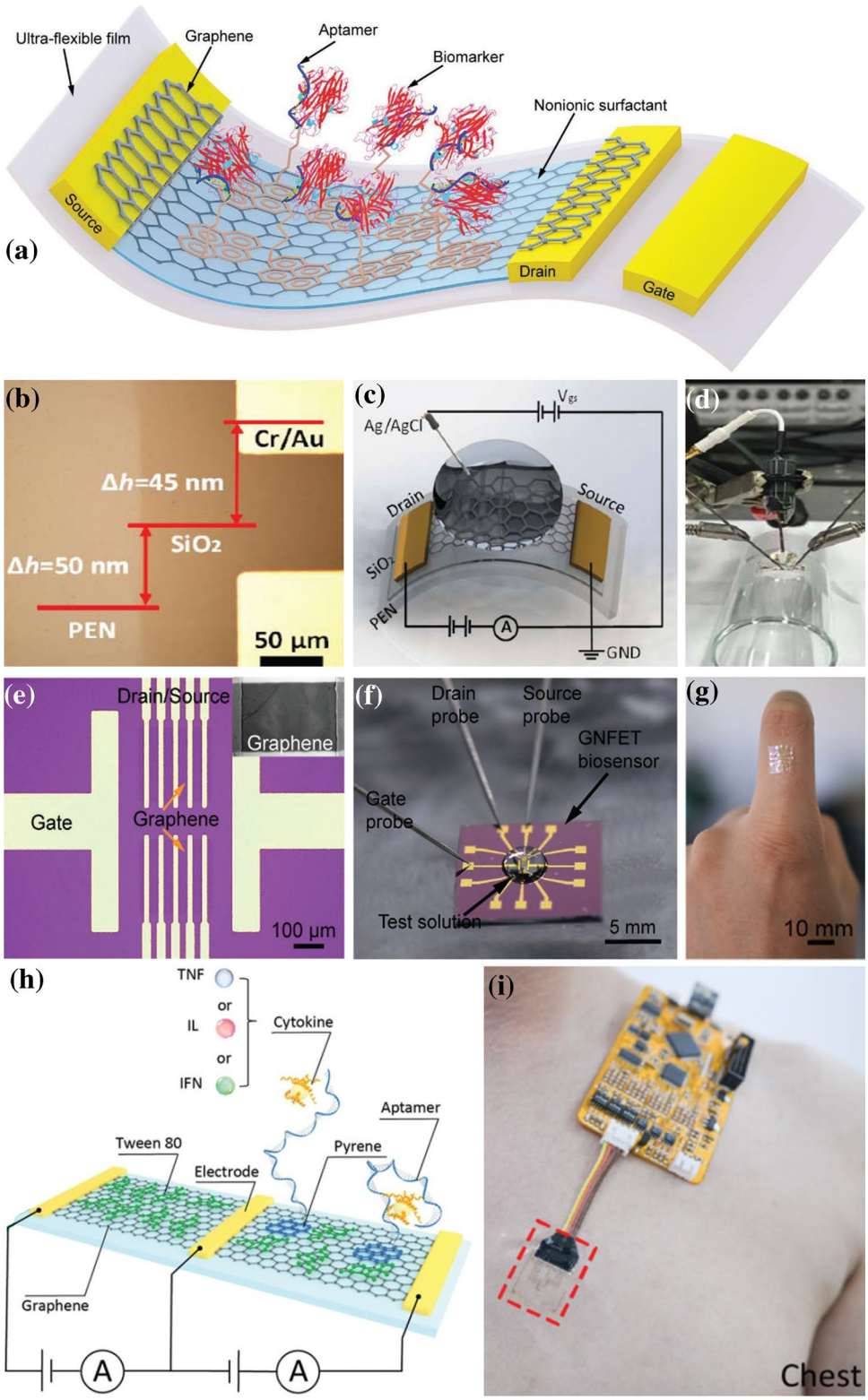

Fig. 9 Aptamers that bind cytokines were used to modify the graphene channel of FETs (a). S/D were made with Cr (2 nm /Au (43 nm) (b) and printed over a SiO_2-coated substrate of the polymer polyethylene naphthalate (PEN) (c), showing good deformability (d). Another similar device uses the biocompatible polymer Mylar (2.5 μm) as the supporting substrate (e–g) and graphene-Nafion composite as a channel. The VDS and VG were supplied using digital source meters, while the IDS was measured (d, f). Since both aptamer and held cytokine (i.e., TNFα or IFNγ) were negatively charged, the union event brings it closer to the channel's surface, changing the properties of the formed EDL and the measured IDS. Further improvement of the platform (detailed in the text) permits its multiplexing (h) for measurements in several biofluids like the sweat in 7 min (i). Reprinted with permission from [113–116, 132]

biosensing of glucose, lactate, and theophylline by chronoamperometry (Fig. 12) [142] using very moderate forces (< 10 N). Notwithstanding, the microneedle systems are challenging to use for aptasensing or immunosensing because of the skin's basal nuclease and protease production and the possibility of initiating chemotaxis and another foreign body reaction where the immune cells are immune like neutrophil degranulate, releasing large quantities of

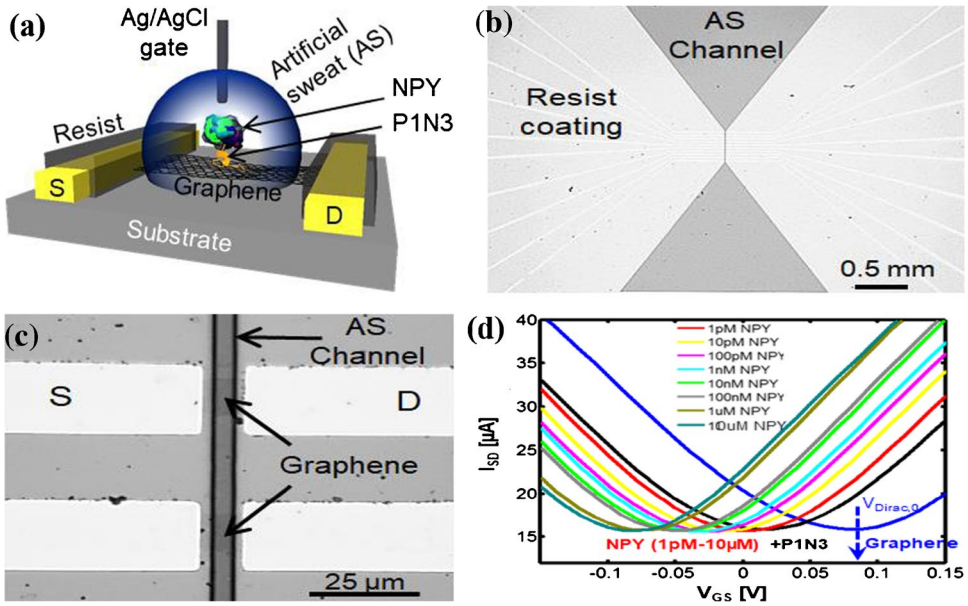

Fig. 10 WEB-FET based on a biorecognition element (BRE) called P1N3 (a). Optical microscope image of the chip (b) and its magnification (c) shows a proper distribution of TiAu S and D electrodes to alter the current I_{SD} at the channel when the customized voltage V_{GS} was applied to generate the transfer curve (d) after immersion into the artificial sweat picked with cortisol. Reprinted with permission from [111]

proteases. The protein adsorption onto electrodes from pseudo-invasive devices like transdermal may induce temporal changes during readout, altering selectivity and signal-to-noise ratio over time. Commonly, there are two mechanisms to ameliorates this problem; i) the modification of the electrode surface with anti-biofouling materials that augment its hydrophilicity, leading to a thin hydration layer that makes the settling of non-specific bindings energetically unfavorable; and ii) the use of high molecular weight molecules to confer steric repulsion. Briefly, these materials had been grouped into four categories: i) polyethylene glycol (PEG)-based materials, ii) zwitterionic polymers, iii) biomimetic materials like hyaluronic acids, and iv) synthetic peptides [143]. Since the protein content of the sweat is relatively low, the biofouling should be minor compared with whole serum or deeper biofluids like ISF. Additionally, microfluidics to separate the device components, a prefiltration or preconcentration of the sample, and differential readout methods also help to reduce the biofouling [125].

Finally, the durability and stability of WEBs should be evaluated because processes like oxidation of the electrode material and variations in temperature, pH, or ionic strength during measurement may lead to false-positive/negative determinations.

Conclusions, remarks, and prospects

World Health Organization (WHO) had proposed nine principles to design wearable health monitoring devices, called REASSURED [144]. Real-time connectivity (i.e., once generated, users immediately obtain results), ii) ease of specimen collection (i.e., noninvasive), iii) affordable, iv) sensitive (i.e., no-false negatives), v) specific (i.e., no-false positives), vi) user-friendly (i.e., straightforward measurement), vii) rapid and robust (i.e., high device stability and short time of response, 15 min to 2 h), viii) equipment-free and environmentally friendly (i.e., autonomous power supply and easy disposable), ix) deliverable to end-users (i.e., cheap). Briefly, the ideal WEB should be noninvasive, autonomous, and stable. Label-free, no calibration requirements, and the capacity to eliminate the biofouling may improve the platforms so that the response time, after biorecognition, is almost immediately and continuously. There are challenges related to mechanics (e.g., noise from motion and strain), size (e.g., Debye screening, time response), sampling system (e.g., sampling frequency), fabrication (e.g., high throughput mass production, ink impurities), energy consumption performance (i.e., the durability of source energy to ensure autonomous running) and long-live after dressing [6, 12, 78, 81–84, 98, 143]. Therefore, it is crucial to consider the applicability of wearable epidermal formats to measure protein biomarkers in terms of issues deliberated across this review. It should be mindful that wearable biosensor remains with its owner (embedded with them). In this fashion, WEBs may exchange information with bedside care equipment (e.g., monitors, electrocardiogram machines, chest X-ray, and computed tomography) by wireless data record. WEBs may also be connected to other records like travel data, vaccination, and medical histories, potentially managed by the Internet of Things (IoT).

Focusing on individual patients, integrating, and analyzing information generated by WEBs expect to improve individualized fitness monitoring, early diseases detection, and better supervision of chronic diseases. For instance, in the monitoring of abuse drugs, wearable sensing may permit

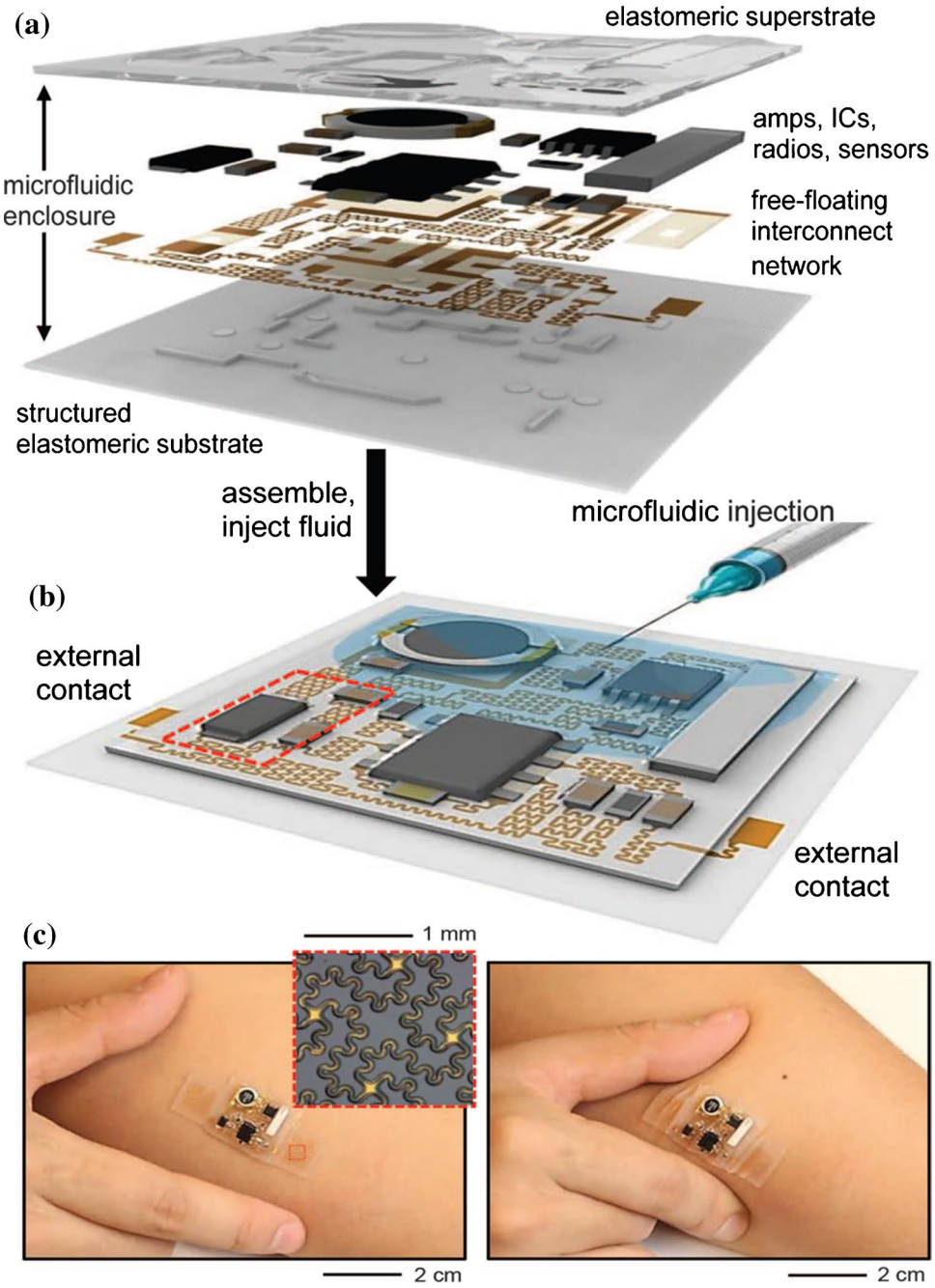

Fig. 11 Hard/soft composite biosensor (a) that uses an elastomeric microfluidic enclosure system to maintain and isolate free-floating interconnected components (b). The device shows high flexibility (c) and may be stretched (left) or twisted (right). Resonant inductive energy transfer is used for wireless power supply. Frequency-modulated RF transmits measured data after a low-noise amplification and filtering of external probe signals. Reprinted with permission from [89]

the toxicologist a remotely continuous register of the vital signs of patients in contrast with levels of the substances in the blood, identifying relapse and tolerance episodes [145]. The crowding of patients into hospitals may be reduced because the integration with telemedicine consultations ensures the medical appointments and a patient's care at his/her home [146]. The possibility of immediate notification to the medical dataset also should enable real-time feedback to the national health systems so that the epidemiology-based decisions may be taken rapidly according to the so actualized results from diagnostic tests' big data. Thus, the use of artificial intelligence (AI) and deep learning (DL) should improve the understanding of healthcare trends to model risk associations and predict outcomes [146]. The last should improve the prevention power of implemented public health strategies [147]. Of course, the generated and integrated information must be stored carefully to avoid hackers and data losses. In this line, the security strategy called blockchain, which does security copies on different peer-to-peer organizations' servers, may protect them by also different cryptographic protocols, making the system reasonably secure [148]. Nowadays, enterprises for real-time

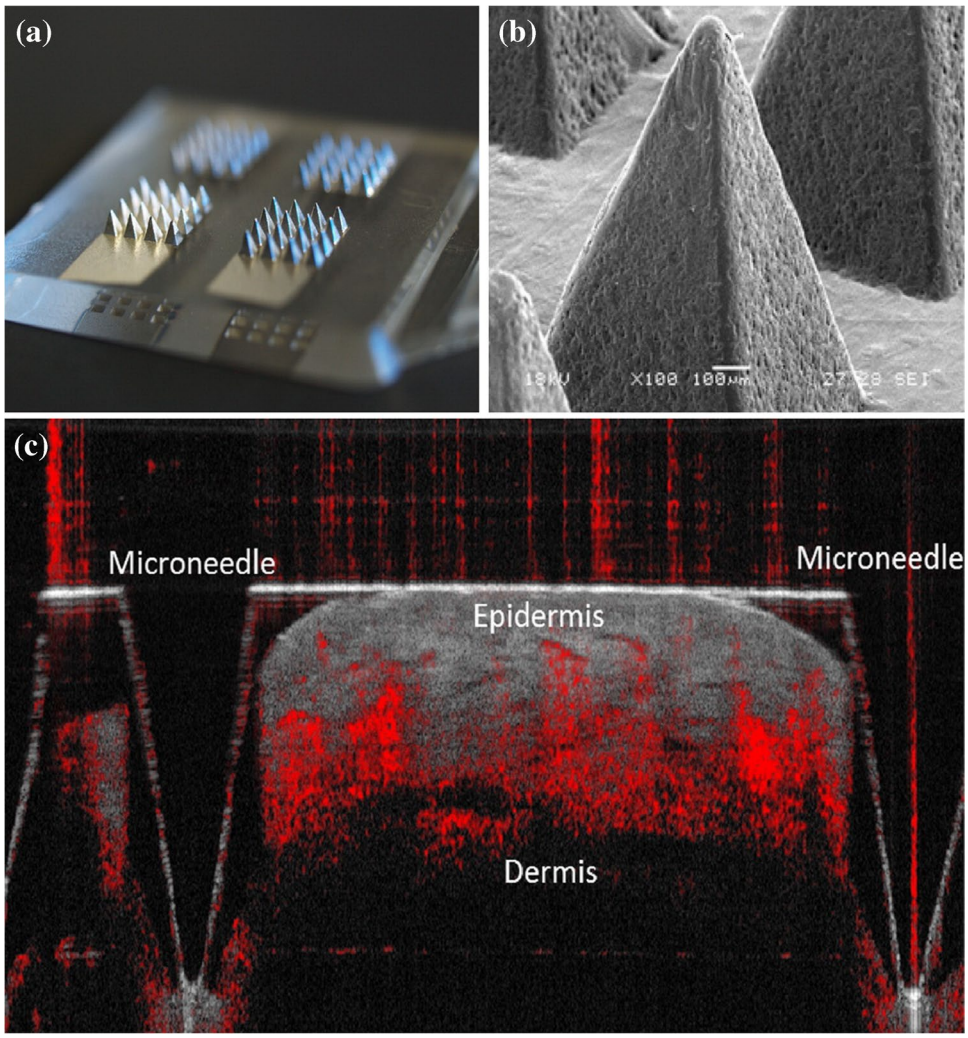

Fig. 12 A polycarbonate microneedle array sputtered with 50 nm Pt (a). The Microneedle surface is regular, as evidenced by the scanning electrochemical microscope images at 100 × (b). The device penetrates ~ 800 µm deep into the skin, as is demonstrated by the optical coherence tomographic image (c). It is possible to fabricate 300-microneedle structures/hour. Reprinted with permission from [142]

COVID-19 records, as World meter, "Our World in Data" (University of Oxford), and COVID-19 Dashboard (Johns Hopkins University), permits tracking the epidemiologic behavior of the pandemic caused by SARS-CoV-2. Most of them are manual records made at medical laboratories around the world. Thus, there is a delay (i.e., days, or even weeks in developing countries) between the actual moment in which the diagnostic test is done (i.e., immunochromatography or PCR for SARS-CoV-2) and the curation data for loading to the "real-time" reports of the system [149]. Despite the referred delay, some studies show the usefulness of this data treatment for design politics that allows the economic reopening without decreasing or maintaining COVID-19 pandemic behavior [150]. In the medical context, continuous real-time monitoring, and connectivity, achieved through devices like electrochemical WEBs, not just will amend the quoted result register delay but also could improve the speed and effectiveness of both the public healthcare policies and the personalized healthcare level of the patients, mainly if WEBs are coupled to digital technologies based on IoT, AI, and DL.

Basic research about the sweat biology is needed. Concretely, the protein partitioning rate as a function of diet, exercise, and diseases progression is required. The disambiguation of release mechanisms will allow separating the basal from pathological levels and eliminate the background introduced by epidermal contamination or apocrine/eccrine sweat gland mixing. The potential utility of sweat protein analytes to evaluate human physiological status also will improve start-up initiatives such as Eccrine Systems, EnLiSense' SWEATSENSER, and CortiWatch. Issues as sweat features according to the patient conditions and sampling techniques, the elimination of byproducts from the epidermis, as well as sebaceous gland secretions and the normal sweat evaporation to avoid cumulation, must be surpassed in research shortly, especially in the real-time monitoring devices like WEBs, in such a way that this kind of promising technology gathers more attention and investment [7, 28, 55, 84].

Acknowledgements DP received funding from MINCIENCIAS through the Project Cod. 111584467470. JO thanks support from The University of Antioquia and the Max Planck Society through the cooperation agreement 566-1, 2014. We thank The Ruta N complex and EPM for hosting the Max Planck Tandem Groups.

Declarations

Conflict of interest The authors declare no competing interests.

References

1. Mann S (1996) Smart clothing: the shift to wearable computing. Commun ACM 39(8):23–24. https://doi.org/10.1145/232014.232021
2. Kaewkannate K, Kim S (2016) A comparison of wearable fitness devices. BMC Public Health 16:433. https://doi.org/10.1186/s12889-016-3059-0
3. Singh AK, Farmer C, Van Den Berg ML, Killington M, Barr CJ (2016) Accuracy of the FitBit at walking speeds and cadences relevant to clinical rehabilitation populations. Disabil Health J 9(2):320–323. https://doi.org/10.1016/j.dhjo.2015.10.011
4. Picard RHJ (1997) Affective wearables. Pers Technol 1:231–240
5. Schmidt P, Reiss A, Dürichen R, Laerhoven KV (2019) Wearable-Based Affect Recognition-A Review. Sensors (Basel), 19(19): 4079. https://doi.org/10.3390/s19194079
6. Lee EK, Kim MK, Lee CH (2019) Skin-Mountable Biosensors and Therapeutics: A Review. Annu Rev Biomed Eng 21:299–323. https://doi.org/10.1146/annurev-bioeng-060418-052315
7. Sonner Z, Wilder E, Heikenfeld J, Kasting G, Beyette F, Swaile D, Sherman F, Joyce J, Hagen J, Kelley-Loughnane N, Naik R (2015) The microfluidics of the eccrine sweat gland, including biomarker partitioning, transport, and biosensing implications. Biomicrofluidics 9(3):031301. https://doi.org/10.1063/1.4921039
8. Someya T, Amagai M (2019) Toward a new generation of smart skins. Nat Biotechnol 37(4):382–388. https://doi.org/10.1038/s41587-019-0079-1
9. Chi YM, Jung TP, Cauwenberghs G (2010) Dry-contact and noncontact biopotential electrodes: methodological review. IEEE Rev Biomed Eng 3:106–119. https://doi.org/10.1109/RBME.2010.2084078
10. Fu Y, Zhao J, Dong Y, Wang X (2020) Dry Electrodes for Human Bioelectrical Signal Monitoring. Sensors (Basel) 20(13):3651. https://doi.org/10.3390/s20133651
11. Yao S, Zhu Y (2016) Nanomaterial-Enabled Dry Electrodes for Electrophysiological Sensing: A Review. JOM 68(4):1145–1155. https://doi.org/10.1007/s11837-016-1818-0
12. Brothers MC, DeBrosse M, Grigsby CC, Naik RR, Hussain SM, Heikenfeld J, Kim SS (2019) Achievements and Challenges for Real-Time Sensing of Analytes in Sweat within Wearable Platforms. Acc Chem Res 52(2):297–306. https://doi.org/10.1021/acs.accounts.8b00555
13. Matsumoto A, Miyahara Y (2013) Current and emerging challenges of field effect transistor based bio-sensing. Nanoscale 5(22):10702–10718. https://doi.org/10.1039/c3nr02703a
14. García M, Batalla P, Escarpa P (2014) Metallic and polymeric nanowires for electrochemical sensing and biosensing. Trends Anal Chem 57:6–22. https://doi.org/10.1016/j.trac.2014.01.004
15. Tamirat Y (2017) The role of nanotechnology in semiconductor industry: Review article. J Mater Sci Nanotechnol 5(2): 202. https://doi.org/10.15744/2348-9812.5.202
16. Han X (2020) Ductile van der Waals materials. Science 369(6503):509. https://doi.org/10.1126/science.abd4527
17. Wei TR, Jin M, Wang Y, Chen H, Gao Z, Zhao K, Qiu P, Shan Z, Jiang J, Li R, Chen L, He J, Shi X (2020) Exceptional plasticity in the bulk single-crystalline van der Waals semiconductor InSe. Science 369(6503):542–545. https://doi.org/10.1126/science.aba9778
18. Mathew M, Radhakrishnan S, Vaidyanathan A, Chakraborty B, Rout CS (2021) Flexible and wearable electrochemical biosensors based on two-dimensional materials: Recent developments. Anal Bioanal Chem 413(3):727–762. https://doi.org/10.1007/s00216-020-03002-y
19. Yin Y, Cheng Z, Wang L, Jin K, Wang W (2014) Graphene, a material for high temperature devices – intrinsic carrier density, carrier drift velocity, and lattice energy. Sci Rep 4(5758):1–6. https://doi.org/10.1038/srep05758
20. Zhang X, Jing Q, Ao S, Schneider GF, Kireev D, Zhang Z, Fu W (2020) Ultrasensitive Field-Effect Biosensors Enabled by the Unique Electronic Properties of Graphene. Small 16(15):e1902820. https://doi.org/10.1002/smll.201902820
21. Brown MA, Crosser MS, Leyden MR, Qi Y (2016) Measurement of high carrier mobility in graphene in an aqueous electrolyte. Appl Phys Lett 109(9):093104. https://doi.org/10.1063/1.4962141
22. Xu J, Fang Y, Chen J (2021) Wearable Biosensors for Non-Invasive Sweat Diagnostics. Biosensors (Basel) 11(8):245. https://doi.org/10.3390/bios11080245
23. Yang A, Yan F (2021) Flexible Electrochemical Biosensors for Health Monitoring. ACS Appl Electron Mater 3(1):53–67. https://doi.org/10.1021/acsaelm.0c00534
24. Lin Y, Chen L, Zhang M, Xie S, Du L, Zhang X, Li H (2021) Eccrine Sweat Gland and Its Regeneration: Current Status and Future Directions. Front Cell Dev Biol 9:667765. https://doi.org/10.3389/fcell.2021.667765
25. Morales M, Pérez D, Correa L, Restrepo L (2016) Evaluation of fibrin-based dermal-epidermal organotypic cultures for in vitro skin corrosion and irritation testing of chemicals according to OECD TG 431 and 439. Toxicol In Vitro 36:89–96. https://doi.org/10.1016/j.tiv.2016.07.010
26. Noël F, Piérard-Franchimont C, Piérard GE, Quatresooz P (2012) Sweaty skin, background and assessments. Int J Dermatol 51(6):647–655. https://doi.org/10.1111/j.1365-4632.2011.05307.x
27. Wilke K, Martin A, Terstegen L, Biel SS (2007) A short history of sweat gland biology. Int J Cosmet Sci 3:169–179. https://doi.org/10.1111/j.1467-2494.2007.00387.x
28. Baker LB (2019) Physiology of sweat gland function: The roles of sweating and sweat composition in human health. Temperature (Austin) 6(3):211–259. https://doi.org/10.1080/23328940.2019.1632145
29. Harshman SW, Pitsch RL, Smith ZK, O'Connor ML, Geier BA, Qualley AV, Schaeublin NM, Fischer MV, Eckerle JJ, Strang AJ, Martin JA (2018) The proteomic and metabolomic characterization of exercise-induced sweat for human performance monitoring: A pilot investigation. PLoS ONE 13(11):e0203133. https://doi.org/10.1371/journal.pone.0203133
30. Serag A, Shakkour Z, Halboup AM, Kobeissy F, Farag MA (2021) Sweat metabolome and proteome: Recent trends in analytical advances and potential biological functions. J Proteomics 246:104310. https://doi.org/10.1016/j.jprot.2021.104310
31. Souza SL, Graça G, Oliva A (2017) Characterization of sweat induced with pilocarpine, physical exercise, and collected passively by metabolomic analysis. Skin Res Technol 24(2):187–195. https://doi.org/10.1111/srt.12412
32. Buono JM, Connolly KP (1992) Increases in sweat rate during exercise: Gland recruitment versus output per gland. J Therm

Biol 15(4–5):267–270. https://doi.org/10.1016/0306-4565(92)90065-N
33. Bovell DL (2018) The evolution of eccrine sweat gland research towards developing a model for human sweat gland function. Exp Dermatol 27(5):544–550. https://doi.org/10.1111/exd.13556
34. Na CH, Sharma N, Madugundu AK, Chen R, Aksit MA, Rosson GD, Cutting GR, Pandey A (2019) Integrated Transcriptomic and Proteomic Analysis of Human Eccrine Sweat Glands Identifies Missing and Novel Proteins. Mol Cell Proteomics 18(7):1382–1395. https://doi.org/10.1074/mcp.RA118.001101
35. Peterson RA, Gueniche A, de Beaumais SA, Breton L, Dalko-Csiba M, Packer NH (2016) Sweating the small stuff: Glycoproteins in human sweat and their unexplored potential for microbial adhesion. Glycobiology 26(3):218–229. https://doi.org/10.1093/glycob/cwv102
36. Buono MJ, Lee NVL, Miller PW (2010) The relationship between exercise intensity and the sweat lactate excretion rate. J Physiol Sci 60(2):103–107. https://doi.org/10.1007/s12576-009-0073-3
37. Maughan RJ, Shirreffs SM (2008) Development of individual hydration strategies for athletes. Int J Sport Nutr Exerc Metab 18(5):457–472. https://doi.org/10.1123/ijsnem.18.5.457
38. Braconnier P, Loncle N, Lourenco J D S, Guérin H, Burnier M, Pruijm M (2018) Sodium concentration of sweat correlates with dietary sodium intake. Journal of Hypertension, 36: pe170. https://doi.org/10.1097/01.hjh.0000539466.81926.69
39. Bates GP, Miller VS (2008) Sweat rate and sodium loss during work in the heat. J Occup Med Toxicol 3:4. https://doi.org/10.1186/1745-6673-3-4
40. Buono MJ, Ball KD, Kolkhorst FW (2007) Sodium ion concentration vs. sweat rate relationship in humans. J Appl Physiol (1985), 103(3): 990–994. https://doi.org/10.1152/japplphysiol.00015.2007
41. Csősz É, Emri G, Kalló G, Tsaprailis G, Tőzsér J (2015) Highly abundant defense proteins in human sweat as revealed by targeted proteomics and label-free quantification mass spectrometry. J Eur Acad Dermatol Venereol 29(10):2024–2031. https://doi.org/10.1111/jdv.13221
42. Raiszadeh MM, Ross MM, Russo PS, Schaepper MA, Zhou W, Deng J, Ng D, Dickson A, Dickson C, Strom M, Osorio C, Soeprono T, Wulfkuhle JD, Petricoin EF, Liotta LA, Kirsh WM (2012) Proteins, Proteomic Analysis of Eccrine Sweat: Implications for the Discovery of Schizophrenia Biomarker. J Proteome Res 11(4):2127–2139. https://doi.org/10.1021/pr2007957
43. Wu C-X, Liu Z-F (2018) Proteomic Profiling of Sweat Exosome Suggests its Involvement in Skin Immunity. J Invest Dermatol 138(1):89–97. https://doi.org/10.1016/j.jid.2017.05.040
44. Jacoby RB, Brahms JC, Ansari SA, Mattai J (2004) Detection and quantification of apocrine secreted odor-binding protein on intact human axillary skin. Int J Cosmet Sci 26(1):37–46. https://doi.org/10.1111/j.0142-5463.2003.00203.x
45. Chen YL, Kuan WH, Liu CL (2020) Comparative Study of the Composition of Sweat from Eccrine and Apocrine Sweat Glands during Exercise and in Heat. Int J Environ Res Public Health 17(10):3377. https://doi.org/10.3390/ijerph17103377
46. Baker LB, Wolfe AS. Physiological mechanisms determining eccrine sweat composition (2020) Eur J Appl Physiol, 120(4):719–752. https://doi.org/10.1007/s00421-020-04323-7
47. Yu Y, Prassas I, Muytjens CMJ, Diamandis EP (2017) Proteomic and peptidomic analysis of human sweat with emphasis on proteolysis. J Proteomics 155:40–48. https://doi.org/10.1016/j.jprot.2017.01.005
48. Adewole OO, Erhabor GE, Adewole TO, Ojo AO, Oshokoya H, Wolfe LM, Prenni JE (2016) Proteomic profiling of eccrine sweat reveals its potential as a diagnostic biofluid for active tuberculosis. Proteomics Clin Appl 10(5):547–553. https://doi.org/10.1002/prca.201500071
49. Heikenfeld J, Jajack A, Rogers J, Gutruf P, Tian L, Pan T, Li R, Khine M, Kim J, Wang J, Kim J (2018) Wearable sensors: modalities, challenges, and prospects. Lab Chip 18(2):217–248. https://doi.org/10.1039/c7lc00914c
50. Marques-Deak A, Cizza G, Eskandari F, Torvik S, Christie IC, Sternberg EM, Phillips TM (2006) Premenopausal, Osteoporosis Women, Alendronate, Depression Study Group. Measurement of cytokines in sweat patches and plasma in healthy women: validation in a controlled study. J Immunol Methods, 315(1–2):99–109. https://doi.org/10.1016/j.jim.2006.07.011
51. Hladek MD, Szanton SL, Cho YE, Lai C, Sacko C, Roberts L, Gill J (2018) Using sweat to measure cytokines in older adults compared to younger adults: A pilot study. J Immunol Methods 454:1–5. https://doi.org/10.1016/j.jim.2017.11.003
52. Russell E, Koren G, Rieder M, Van Uum SH (2014) The detection of cortisol in human sweat: implications for measurement of cortisol in hair. Ther Drug Monit 36(1):30–34. https://doi.org/10.1097/FTD.0b013e31829daa0a
53. Jia M, Chew WM, Feinstein Y, Skeath P, Sternberg EM (2016) Quantification of cortisol in human eccrine sweat by liquid chromatography - tandem mass spectrometry. Analyst 141(6):2053–2060. https://doi.org/10.1039/c5an02387d
54. Pearlmutter P, DeRose G, Samson C, Linehan N, Cen Y, Begdache L, Won D, Koh A (2020) Sweat and saliva cortisol response to stress and nutrition factors. Sci Rep 10(1):19050. https://doi.org/10.1038/s41598-020-75871-3
55. Jagannath B, Lin KC, Pali M, Sankhala D, Muthukumar S, Prasad S (2021) Temporal profiling of cytokines in passively expressed sweat for detection of infection using wearable device. Bioeng Transl Med 6(3):e10220. https://doi.org/10.1002/btm2.10220
56. Torrente-Rodríguez RM, Tu J, Yang Y, Min J, Wang M, Song Y, Yu Y, Xu C, Ye C, IsHak WW, Gao W (2020) Investigation of cortisol dynamics in human sweat using a graphene-based wireless mHealth system. Matter 2(4):921–937. https://doi.org/10.1016/j.matt.2020.01.021
57. Upasham S, Churcher NKM, Rice P, Prasad S (2021) Sweating Out the Circadian Rhythm: A Technical Review. ACS Sens 6(3):659–672. https://doi.org/10.1021/acssensors.0c02622
58. Dai X, Okazaki H, Hanakawa Y, Murakami M, Tohyama M, Shirakata Y, Sayama K (2013) Eccrine sweat contains IL-1α, IL-1β and IL-31 and activates epidermal keratinocytes as a danger signal. PLoS ONE 8(7):e67666. https://doi.org/10.1371/journal.pone.0067666
59. Lee DY, Kim E, Choi MH (2015) Technical and clinical aspects of cortisol as a biochemical marker of chronic stress. BMB Rep 48(4):209–216. https://doi.org/10.5483/bmbrep.2015.48.4.275
60. Pérez DJ, Patiño EB, Orozco J (2021) Electrochemical Nanobiosensors as Point-of-care Testing Solution to Cytokines Measurement Limitations. Electroanalysis, 1-29. https://doi.org/10.1002/elan.202100237
61. Baker LB (2017) Sweating Rate and Sweat Sodium Concentration in Athletes: A Review of Methodology and Intra/Interindividual Variability. Sports Med 47(Suppl 1):111–128. https://doi.org/10.1007/s40279-017-0691-5
62. Basu S, Mitra M, Ghosh A (2013) Evaluation of sweat production by pilocarpine iontophoresis: a noninvasive screening tool for hypohidrosis in ectodermal dysplasia. Indian J Clin Biochem 28(4):433–435. https://doi.org/10.1007/s12291-013-0334-z
63. Hancock J (2007) Pilocarpine. In: Enna SJ, Bylund DB (eds) xPharm: The Comprehensive Pharmacology Reference. Elsevier, Johnson City, pp 1–7
64. Vairo D, Bruzzese L, Marlinge M, Fuster L, Adjriou N, Kipson N, Brunet P, Cautela J, Jammes Y, Mottola G, Burtey S, Ruf J, Guieu R, Fenouillet E (2017) Towards Addressing the

Body Electrolyte Environment via Sweat Analysis: Pilocarpine Iontophoresis Supports Assessment of Plasma Potassium Concentration. Sci Rep 7(1):11801. https://doi.org/10.1038/s41598-017-12211-y
65. Cunningham DD (2010) Transdermal Microfluidic Continuous Monitoring Systems. In: Cunningham DD, Stenken JA (eds) In Vivo Glucose Sensing. John Wiley & Sons, Hoboken, New Jersey, pp 191–216
66. Kim J, Sempionatto JR, Imani S, Hartel MC, Barfidokht A, Tang G, Campbell AS, Mercier PP, Wang J (2018) Simultaneous Monitoring of Sweat and Interstitial Fluid Using a Single Wearable Biosensor Platform. Adv Sci (Weinh) 5(10):1800880. https://doi.org/10.1002/advs.201800880
67. Sempionatto JR, Lin M, Yin L, De la Paz E, Pei K, Sonsa-Ard T, de Loyola Silva AN, Khorshed AA, Zhang F, Tostado N, Xu S, Wang J (2021) An epidermal patch for the simultaneous monitoring of haemodynamic and metabolic biomarkers. Nat Biomed Eng 5(7):737–748. https://doi.org/10.1038/s41551-021-00685-1
68. Ita K (2017) Recent progress in transdermal sonophoresis. Pharm Dev Technol 22(4):458–466. https://doi.org/10.3109/10837450.2015.1116566
69. Liu C, Xu T, Wang D, Zhang X (2020) The role of sampling in wearable sweat sensors. Talanta 212:120801. https://doi.org/10.1016/j.talanta.2020.120801
70. Vashist SK (2012) Non-invasive glucose monitoring technology in diabetes management: a review. Anal Chim Acta 750:16–27. https://doi.org/10.1016/j.aca.2012.03.043
71. Emaminejad S, Gao W, Wu E, Davies ZA, Yin Yin Nyein H, Challa S, Ryan SP, Fahad HM, Chen K, Shahpar Z, Talebi S, Milla C, Javey A, Davis RW (2017) Autonomous sweat extraction and analysis applied to cystic fibrosis and glucose monitoring using a fully integrated wearable platform. Proc Natl Acad Sci U S A 114(18):4625–4630. https://doi.org/10.1073/pnas.1701740114
72. Hojaiji H, Zhao Y, Gong MC, Mallajosyula M, Tan J, Hojaiji H, Lin HAM, Lin S, Milla C, Madnib AM, Emaminejad S (2020) An autonomous wearable system for diurnal sweat biomarker data acquisition. Lab Chip 20(24):4582–4591. https://doi.org/10.1039/D0LC00820F
73. Kim J, Jeerapan I, Imani S, Cho TN, Bandodkar A, Cinti S, Mercier PP, Wang J (2016) Noninvasive Alcohol Monitoring Using a Wearable Tattoo-Based Iontophoretic-Biosensing System. ACS Sens 1(8):1011–1019. https://doi.org/10.1021/acssensors.6b00356
74. Yang Y, Gao W (2019) Wearable and flexible electronics for continuous molecular monitoring. Chem Soc Rev 48(6):1465–1491. https://doi.org/10.1039/c7cs00730b
75. Miyamoto A, Lee S, Cooray NF, Lee S, Mori M, Matsuhisa N, Jin H, Yoda L, Yokota T, Itoh A, Sekino M, Kawasaki H, Ebihara T, Amagai M, Someya T (2017) Inflammation-free, gas-permeable, lightweight, stretchable on-skin electronics with nanomeshes. Nat Nanotechnol 12(9):907–913. https://doi.org/10.1038/nnano.2017.125
76. Béraud A, Sauvage M, Bazán CM, Tie M, Bencherif A, Bouilly D (2021) Graphene field-effect transistors as bioanalytical sensors: design, operation and performance. Analyst 146(2):403–428. https://doi.org/10.1039/d0an01661f
77. Zheng Z, Zhang H, Zhai T, Xia F (2020) Overcome Debye Length Limitations for Biomolecule Sensing Based on Field Effective Transistors. Chin J Chem 39(4):999–1008. https://doi.org/10.1002/cjoc.202000584
78. Bandodkar AJ, Jeerapan I, Wang J (2016) Wearable Chemical Sensors: Present Challenges and Future Prospects. ACS Sens 1(5):464–482. https://doi.org/10.1021/acssensors.6b00250
79. Chaniotakis N, Fouskaki M (2014) Bio-chem-FETs: field effect transistors for biological sensing. In: Schaudies RP (ed) Biological Identification: DNA Amplification and Sequencing, Optical Sensing, Lab-On-chip and Portable Systems, Cambridge, Woodhead Publishing, pp 194-219
80. Lee YH, Jang M, Lee MY, Kweon OY, Oh JH (2017) Flexible Field-Effect Transistor-Type Sensors Based on Conjugated Molecules. Chem 3(5):724–763. https://doi.org/10.1016/j.chempr.2017.10.005
81. Li M-Z, Han S-T, Zhou Y (2020) Recent Advances in Flexible Field-Effect Transistors toward Wearable Sensors. Sensors Adv Intell Syst 1(2000113):1–26. https://doi.org/10.1002/aisy.202000113
82. Bariya M, Nyein H Y Y, Javey A (2018) Wearable sweat sensors. Nat Electron, 1: 160-171. https://doi.org/10.1038/s41928-018-0043-y
83. Takaloo S, Zand MM (2021) Wearable electrochemical flexible biosensors: With the focus on affinity biosensors. Sens Bio-Sens Res 32(100403):1–11. https://doi.org/10.1016/j.sbsr.2021.100403
84. Kim J, Campbell AS, de Ávila BE, Wang J (2019) Wearable biosensors for healthcare monitoring. Nat Biotechnol 37(4):389–406. https://doi.org/10.1038/s41587-019-0045-y
85. Shetti NP, Mishra A, Basu S, Mascarenhas RJ, Kakarla RR, Aminabhavi TM (2020) Skin-Patchable Electrodes for Biosensor Applications: A Review. ACS Biomater Sci Eng 6(4):1823–1835. https://doi.org/10.1021/acsbiomaterials.9b01659
86. Lee EK, Baruah RK, Bhamra H, Kim YJ, Yoo H (2021) Recent advances in electrode development for biomedical applications. Biomed Eng Lett 11(2):107–115. https://doi.org/10.1007/s13534-021-00189-6
87. Wang X, Liu Y, Chen Q, Yan Y, Rao Z, Lin Z, Chen H, Guo T (2021) Recent advances in stretchable field-effect transistors. J Mater Chem C 9(25):7796–7828. https://doi.org/10.1039/D1TC01082D
88. Kim DH, Lu N, Ma R, Kim YS, Kim RH, Wang S, Wu J, Won SM, Tao H, Islam A, Yu KJ, Kim TI, Chowdhury R, Ying M, Xu L, Li M, Chung HJ, Keum H, McCormick M, Liu P, Zhang YW, Omenetto FG, Huang Y, Coleman T, Rogers JA (2011) Epidermal electronics. Science 333(6044):838–843. https://doi.org/10.1126/science.1206157
89. Xu S, Zhang Y, Jia L, Mathewson KE, Jang KI, Kim J, Fu H, Huang X, Chava P, Wang R, Bhole S, Wang L, Na YJ, Guan Y, Flavin M, Han Z, Huang Y, Rogers JA (2014) Soft microfluidic assemblies of sensors, circuits, and radios for the skin. Science 344(6179):70–74. https://doi.org/10.1126/science.1250169
90. Ortega L, Llorella A, Esquivel JP, Sabaté N (2019) Self-powered smart patch for sweat conductivity monitoring. Microsyst Nanoeng 5:3. https://doi.org/10.1038/s41378-018-0043-0
91. Rovira M, Fernández-Sánchez C, Jiménez-Jorquera C (2021) Hybrid Technologies Combining Solid-State Sensors and Paper/Fabric Fluidics for Wearable Analytical Devices. Biosensors (Basel) 11(9):303. https://doi.org/10.3390/bios11090303
92. Yu Y, Nassar J, Xu C, Min J, Yang Y, Dai A, Doshi R, Huang A, Song Y, Gehlhar R, Ames AD, Gao W (2020) Biofuel-powered soft electronic skin with multiplexed and wireless sensing for human-machine interfaces. Sci Robot, 22;5(41): eaaz7946. https://doi.org/10.1126/scirobotics.aaz7946
93. Chortos A, Koleilat GI, Pfattner R, Kong D, Lin P, Nur R, Lei T, Wang H, Liu N, Lai YC, Kim MG, Chung JW, Lee S, Bao Z (2016) Mechanically Durable and Highly Stretchable Transistors Employing Carbon Nanotube Semiconductor and Electrodes. Adv Mater 28(22):4441–4448. https://doi.org/10.1002/adma.201501828
94. Moheimani R, Aliahmad N, Aliheidari N, Agarwal M, Dalir H (2021) Thermoplastic polyurethane flexible capacitive proximity sensor reinforced by CNTs for applications in the creative industries. Sci Rep 11(1):1104. https://doi.org/10.1038/s41598-020-80071-0

95. He W, Wang C, Wang H, Jian M, Lu W, Liang X, Zhang X, Yang F, Zhang Y (2019) Integrated textile sensor patch for real-time and multiplex sweat analysis. Sci Adv, 5(11): eaax0649. https://doi.org/10.1126/sciadv.aax0649
96. Ma Z (2011) An electronic second skin. Science, 333 (6044): 830-831. https://doi.org/10.1126/science.1209094
97. Voulgari E, Krummenacher F, Kayal M (2021) ANTIGONE: A Programmable Energy-Efficient Current Digitizer for an ISFET Wearable Sweat Sensing System. Sensors (Basel) 21(6):2074. https://doi.org/10.3390/s21062074
98. Gu Y, Zhang T, Chen H, Wang F, Pu Y, Gao C, Li S (2019) Mini Review on Flexible and Wearable Electronics for Monitoring Human Health Information. Nanoscale Res Lett 14(1):263. https://doi.org/10.1186/s11671-019-3084-x
99. Manjakkal L, Yin L, Nathan A, Wang J, Dahiya R. Energy Autonomous Sweat-Based Wearable Systems. Adv Mater, 33(35): e2100899. https://doi.org/10.1002/adma.202100899
100. García C, Libu M, Dahiya R (2019) Energy autonomous electronic skin. npj Flex Electron, 3(1): 1–24. https://doi.org/10.1038/s41528-018-0045-x
101. Munje RD, Muthukumar S, Jagannath B, Prasad S (2017) A new paradigm in sweat based wearable diagnostics biosensors using Room Temperature Ionic Liquids (RTILs). Sci Rep 7(1950):1–12. https://doi.org/10.1038/s41598-017-02133-0
102. Churcher NKM, Upasham S, Rice P, Bhadsavle S, Prasad S (2020) Neuropeptide Y Development of a flexible, sweat-based neuropeptide Y detection platform. RSC Adv 10(39):23173–23186. https://doi.org/10.1039/D0RA03729J
103. Upasham SS, Thai K, Muthyala R, Prasad S (2020) Flexible, low volume detection of chronobiology biomarkers from human sweat. Analyst 145(3):784–796. https://doi.org/10.1039/c9an01968e
104. Ganguly A, Lin KC, Muthukumar S, Prasad S (2021) Autonomous, Real-Time Monitoring Electrochemical Aptasensor for Circadian Tracking of Cortisol Hormone in Sub-microliter Volumes of Passively Eluted Human Sweat. ACS Sens 6(1):63–72. https://doi.org/10.1021/acssensors.0c01754
105. Rice P, Upasham S, Jagannath B, Manuel R, Pali M, Prasad S (2019) CortiWatch: watch-based cortisol tracker. Future Sci OA, 5(9): FSO416. https://doi.org/10.2144/fsoa-2019-0061
106. Upasham S, Prasad S (2020) SLOCK (sensor for circadian clock): passive sweatbased chronobiology tracker. Lab Chip 20(11):1947–1960. https://doi.org/10.1039/d0lc00134a
107. Upasham S, Osborne O, Prasad S (2021) Demonstration of sweat-based circadian diagnostic capability of SLOCK using electrochemical detection modalities. RSC Adv 11(13):7750–7765. https://doi.org/10.1039/D0RA10561A
108. Upasham S, Prasad S (2021) Tuning SLOCK toward Chronic Disease Diagnostics and Management: Label-free Sweat Interleukin-31 Detection. ACS Omega 6(31):20422–20432. https://doi.org/10.1021/acsomega.1c02414
109. Jagannath B, Lin KC, Pali M, Sankhala D, Muthukumar S, Prasad S. A Sweat-based Wearable Enabling Technology for Real-time Monitoring of IL-1β and CRP as Potential Markers for Inflammatory Bowel Disease. Inflamm Bowel Dis, 26(10): 1533–1542. https://doi.org/10.1093/ibd/izaa191
110. Parlak O, Keene ST, Marais A, Curto VF, Salleo A (2018) Molecularly selective nanoporous membrane-based wearable organic electrochemical device for noninvasive cortisol sensing. Sci Adv, 20;4(7): eaar2904. https://doi.org/10.1126/sciadv.aar2904
111. Islam AE, Martineau R, Crasto CM, Kim H, Rao RS, Maruyama B, Kim SS, Drummy LF (2020) Graphene-Based Electrolyte-Gated Field-Effect Transistors for Potentiometrically Sensing Neuropeptide Y in Physiologically Relevant Environments. ACS Appl Nano Mater 3(6):5088–5097. https://doi.org/10.1021/acsanm.0c00353
112. Kim S, Xing L, Islam AE, Hsiao MS, Ngo Y, Pavlyuk OM, Martineau RL, Hampton CM, Crasto C, Slocik J, Kadakia MP, Hagen JA, Kelley-Loughnane N, Naik RR, Drummy LF (2019) In Operando Observation of Neuropeptide Capture and Release on Graphene Field-Effect Transistor Biosensors with Picomolar Sensitivity. ACS Appl Mater Interfaces 11(15):13927–13934. https://doi.org/10.1021/acsami.8b20498
113. Hao Z, Wang Z, Li Y, Zhu Y, Wang X, De Moraes CG, Pan Y, Zhao X, Lin Q (2018) Measurement of cytokine biomarkers using an aptamer-based affinity graphene nanosensor on a flexible substrate toward wearable applications. Nanoscale 10(46):21681–21688. https://doi.org/10.1039/c8nr04315a
114. Wang Z, Hao Z, Yu S, De Moraes CG, Suh LH, Zhao X, Lin Q (019) An Ultraflexible and Stretchable Aptameric Graphene Nanosensor for Biomarker Detection and Monitoring. Adv Funct Mater, 29(44): 1905202. https://doi.org/10.1002/adfm.201905202
115. Wang Z, Hao Z, Yu S, Huang C, Pan Y, Zhao X (2020) A Wearable and Deformable Graphene-Based Affinity Nanosensor for Monitoring of Cytokines in Biofluids. Nanomaterials (Basel) 10(8):1503. https://doi.org/10.3390/nano10081503
116. Wang Z, Hao Z, Wang X, Huang C, Lin Q, Zhao X, Pan Y (2020) A Flexible and Regenerative Aptameric Graphene-Nafion Biosensor for Cytokine Storm Biomarker Monitoring in Undiluted Biofluids toward Wearable Applications. Adv Funct Mater 31(4):2005958. https://doi.org/10.1002/adfm.202005958
117. Zhang Y, Liu CY, Chen WC, Shi YC, Wang CM, Lin S, He HF (2021) Regulation of neuropeptide Y in body microenvironments and its potential application in therapies: a review. Cell Biosci 11(1):151. https://doi.org/10.1186/s13578-021-00657-7
118. Cizza G, Marques AH, Eskandari F, Christie IC, Torvik S, Silverman MN, Phillips TM, Sternberg EM; POWER Study Group (2008) Elevated neuroimmune biomarkers in sweat patches and plasma of premenopausal women with major depressive disorder in remission: the POWER study. Biol Psychiatry, 64(10): 907-11. https://doi.org/10.1016/j.biopsych.2008.05.035
119. Sadighbayan D, Hasanzadeh M, Ghafar-Zadeh E (2020) Biosensing based on field-effect transistors (FET): Recent progress and challenges. Trends Analyt Chem 133:116067. https://doi.org/10.1016/j.trac.2020.116067
120. Veres J, Ogier S, Lloyd G, de Leeuw D (2004) Gate Insulators in Organic Field-Effect Transistors. Chem Mater 16(23):4543–4555. https://doi.org/10.1021/cm049598q
121. Kaisti M (2017) Detection principles of biological and chemical FET sensors. Biosens Bioelectron 98:437–448. https://doi.org/10.1016/j.bios.2017.07.010
122. Wang YY, Burke PJ (2013) A large-area and contamination-free graphene transistor for liquidgated sensing applications. Appl Phys Lett 103:052103. https://doi.org/10.1063/1.4816764
123. Rajan NK, Brower K, Duan X, Reed MA (2014) Limit of detection of field effect transistor biosensors: Effects of surface modification. Appl Phys Lett 104(8):084106. https://doi.org/10.1063/1.4867025
124. Ahn J-H, Bongsik C, Choi S-J (2020) Understanding the signal amplification in dual-gate FET-based biosensors. J Appl Phys 128(18):184502. https://doi.org/10.1063/5.0010136
125. Rollo S, Rani D, Olthuis W, Pascual García C (2019) The influence of geometry and other fundamental challenges for biosensing with field effect transistors. Biophys Rev 11(5):757–763. https://doi.org/10.1007/s12551-019-00592-5
126. Nakata S, Arie T, Akita S, Takei K (2017) Wearable, flexible, and multifunctional healthcare device with an ISFET chemical sensor for simultaneous sweat pH and skin temperature monitoring. ACS Sens 2(3):443–448. https://doi.org/10.1021/acssensors.7b00047
127. Bhatt K, Kumar S, Tripathi C C (2020) High-performance ultra-low leakage current graphene-based screen-printed field-effect

transistor on paper substrate. Pramana – J Phys, 94(31): 1–4. https://doi.org/10.1007/s12043-019-1906-0
128. Q Liu Q, Zhao C, Chen M, Liu Y, Zhao Z, Wu F, Li Z, Weiss PS, Andrews AM, Zhou C (2020) Flexible Multiplexed In2O3 Nanoribbon Aptamer-Field-Effect Transistors for Biosensing. iScience, 23(9): 101469. https://doi.org/10.1016/j.isci.2020.101469
129. Gebbie MA, Smith AM, Dobbs HA, Lee AA, Warr GG, Banquy X, Valtiner M, Rutland MW, Israelachvili JN, Perkin S, Atkin R (2017) Long range electrostatic forces in ionic liquids. Chem Commun (Camb) 53(7):1214–1224. https://doi.org/10.1039/c6cc08820a
130. Kim DJ, Sohn IY, Jung JH, Yoon OJ, Lee NE, Park JS (2013) Reduced graphene oxide field-effect transistor for label-free femtomolar protein detection. Biosens Bioelectron 41:621–626. https://doi.org/10.1016/j.bios.2012.09.040
131. Dwived P, Kranti A (2017) Applicability of Transconductance-to-Current Ratio (gm/Ids) as a Sensing Metric for Tunnel FET Biosensors. IEEE Sens J 17(4):1030–1036. https://doi.org/10.1109/JSEN.2016.2640192
132. Hao Z, Luo Y, Huang C, Wang Z, Song G, Pan Y, Zhao X, Liu S (2021) An Intelligent Graphene-Based Biosensing Device for Cytokine Storm Syndrome Biomarkers Detection in Human Biofluids. Small 17(29):e2101508. https://doi.org/10.1002/smll.202101508
133. Park H, Park W, Lee CH (2021) Electrochemically active materials and wearable biosensors for the in situ analysis of body fluids for human healthcare. NPG Asia Materials 13(23):1–14. https://doi.org/10.1038/s41427-020-00280-x
134. Stern E, Wagner R, Sigworth FJ, Breaker R, Fahmy TM, Reed MA (2007) Importance of the Debye screening length on nanowire field effect transistor sensors. Nano Lett 7(11):3405–3409. https://doi.org/10.1021/nl071792z
135. Shoorideh K, Chui CO (2014) On the origin of enhanced sensitivity in nanoscale FET-based biosensors. Proc Natl Acad Sci U S A 111(14):5111–5116. https://doi.org/10.1073/pnas.1315485111
136. Dickinson EJF, Compton RG (2009) Diffuse Double Layer at Nanoelectrodes. J Phys Chem C 113(41):17585–17589. https://doi.org/10.1021/jp906404h
137. Chu CH, Sarangadharan I, Regmi A, Chen YW, Hsu CP, Chang WH, Lee GY, Chyi JI, Chen CC, Shiesh SC, Lee GB, Wang YL (2017) Beyond the Debye length in high ionic strength solution: direct protein detection with field-effect transistors (FETs) in human serum. Sci Rep 7(1):5256. https://doi.org/10.1038/s41598-017-05426-6
138. Sheehan PE, Whitman LJ (2005) Detection limits for nanoscale biosensors. Nano Lett 5(4):803–807. https://doi.org/10.1021/nl050298x
139. Naira PR, Alam MA (2006) Performance limits of nanobiosensors. Appl Phys Lett 88(23):233120. https://doi.org/10.1063/1.2211310
140. Squires TM, Messinger RJ, Manalis SR (2008) Making it stick: convection, reaction and diffusion in surface-based biosensors. Nat Biotechnol 26(4):417–426. https://doi.org/10.1038/nbt1388
141. Jin D S, Brightbill E L, Vogel E M. General model for mass transport to planar and nanowire biosensor surfaces. J Appl Phys, 125(11): 114502, https://doi.org/10.1063/1.5084253
142. Sharma S, Saeed A, Johnson C, Gadegaard N, Cass AE (2017) Rapid, low cost prototyping of transdermal devices for personal healthcare monitoring. Sens Biosensing Res 13:104–108. https://doi.org/10.1016/j.sbsr.2016.10.004
143. Liu N, Xu Z, Morrin A, Luo X (2019) Low fouling strategies in electrochemical biosensors targeting disease biomarkers. Anal Methods 11(6):702–711. https://doi.org/10.1039/C8AY02674B
144. Bernabé-Ortiz A, Zafra-Tanaka JH, Moscoso-Porras M, Sampath R, Vetter B, Miranda JJ, Beran D (2021) Diagnostics and monitoring tools for noncommunicable diseases: a missing component in the global response. Global Health 17(1):26. https://doi.org/10.1186/s12992-021-00676-6
145. Chai PR (2016) Wearable Devices and Biosensing: Future Frontiers. J Med Toxicol 12(4):332–334. https://doi.org/10.1007/s13181-016-0569-1
146. Ting DSW, Carin L, Dzau V, Wong TY (2020) Digital technology and COVID-19. Nat Med 26(4):459–461. https://doi.org/10.1038/s41591-020-0824-5
147. Hosseinifard M, Naghdi T, Morales-Narváez E, Golmohammadi H (2021) Toward Smart Diagnostics in a Pandemic Scenario: COVID-19. Front Bioeng Biotechnol 9:637203. https://doi.org/10.3389/fbioe.2021.637203
148. van Rossum J (2017) Blockchain for Research: Perspectives on a New Paradigm for Scholarly Communication. Digital Science. https://doi.org/10.6084/m9.figshare.5607778
149. Dong E, Du H, Gardner L (2020) An interactive web-based dashboard to track COVID-19 in real time. Lancet Infect Dis 20(5):533–534. https://doi.org/10.1016/S1473-3099(20)30120-1
150. Shonchoy AS, Ishtiaq KS, Talukder S, Ahmed NU, Chowdhury R (2021) A novel index-based decision support toolkit for safe reopening following a generalized lockdown in low and middle-income countries. Sci Rep 11(1):14108. https://doi.org/10.1038/s41598-021-93415-1